AFRL-AFOSR-JP-TR-2020-0007

Investigating Ionospheric Heat Sources and Resultant Thermospheric Responses

Ildiko Horvath
THE UNIVERSITY OF QUEENSLAND
UNIVERSITY OF QUEENSLAND
BRISBANE, 4072
AU

07/11/2020
Final Report

Air Force Research Laboratory
Air Force Office of Scientific Research
Asian Office of Aerospace Research and Development
Unit 45002, APO AP 96338-5002

REPORT DOCUMENTATION PAGE

Form Approved
OMB No. 0704-0188

1. REPORT DATE *(DD-MM-YYYY)*	2. REPORT TYPE	3. DATES COVERED *(From - To)*
11-07-2020	Final	29 Sep 2017 to 28 Jan 2020

4. TITLE AND SUBTITLE
Investigating Ionospheric Heat Sources and Resultant Thermospheric Responses

5a. CONTRACT NUMBER

5b. GRANT NUMBER
FA2386-17-1-4109

5c. PROGRAM ELEMENT NUMBER
61102F

6. AUTHOR(S)
Ildiko Horvath

5d. PROJECT NUMBER

5e. TASK NUMBER

5f. WORK UNIT NUMBER

7. PERFORMING ORGANIZATION NAME(S) AND ADDRESS(ES)
THE UNIVERSITY OF QUEENSLAND
UNIVERSITY OF QUEENSLAND
BRISBANE, 4072 AU

8. PERFORMING ORGANIZATION REPORT NUMBER

9. SPONSORING/MONITORING AGENCY NAME(S) AND ADDRESS(ES)
AOARD
UNIT 45002
APO AP 96338-5002

10. SPONSOR/MONITOR'S ACRONYM(S)
AFRL/AFOSR IOA

11. SPONSOR/MONITOR'S REPORT NUMBER(S)
AFRL-AFOSR-JP-TR-2020-0007

12. DISTRIBUTION/AVAILABILITY STATEMENT
A DISTRIBUTION UNLIMITED: PB Public Release

13. SUPPLEMENTARY NOTES

14. ABSTRACT
During this project, the team conducted detailed investigations on various complex geophysical processes occurring in the coupled system of solar wind, magnetosphere, ionosphere, and thermosphere (SW-M-I-T). The main goal was to unravel some of the physical processes that (i) underlie the development of localized neutral density increases and (ii) occur in the coupled SW-M-I-T system in order to better understand how and where the heat sources fueling upwelling and leading to localized neutral density increases developed. By utilizing the innovative methodologies of interplanetary magnetic field parameterization and flow channel (FC) classification, they were able to investigate various geophysical processes that had not been understood well and/or been less investigated. The geophysical processes investigated occurred at various geomagnetic activity levels, ranging from moderate storms to superstorms, and sometimes were driven by solar-wind Alfven waves propagating away from the sun. Their new results and findings have led to the unravelling of near-pole electromagnetic energy deposition via various types of FCs, ASAID development during magnetically quiet times, and large sub-auroral polarization streams (SAPS) FC development under superstorm conditions. Highlighted are first ASAID detections by utilizing polar data and first demonstrations of large-scale TIDs enhancing SAPS FCs and SAPS_WS (i.e., the structured version of SAPS). These new results and finding contribute to the better understanding of many basic geophysical processes by explaining fundamental multiple inter-relationships and configurations.

15. SUBJECT TERMS
Ionosphere, Heating, Thermosphere

16. SECURITY CLASSIFICATION OF:			17. LIMITATION OF ABSTRACT	18. NUMBER OF PAGES	19a. NAME OF RESPONSIBLE PERSON
a. REPORT	b. ABSTRACT	c. THIS PAGE			CHEN, JERMONT
Unclassified	Unclassified	Unclassified	SAR		19b. TELEPHONE NUMBER *(Include area code)* 315-227-7007

Final Report for AOARD Grant FA2386-17-1-4109
Project Title: Investigating Ionospheric Heat Sources and Resultant Thermospheric Responses
Date: 5 February 2020

Name of Principal Investigators (PI and Co-PIs): Dr Ildiko HORVATH
- Email address: ihorvath@itee.uq.edu.au
- Institution: The University of Queensland; School of Information Technology and Electrical Engineering
- Mailing Address: The University of Queensland, St. Lucia, Brisbane, QLD, Australia
- Phone: +61 7 336 51643
- Fax: +61 7 33654999

AOARD Program Manager: Dr Sheena Winder
Period of Performance: 30 September 2017 to 28 January 2020

Abstract:

During this 2-year-4-month project, we have conducted detailed investigations on various complex geophysical processes occurring in the coupled system of solar wind, magnetosphere, ionosphere, and thermosphere (SW-M-I-T). Our main goal was to unravel some of the physical processes that (i) underlie the development of localized neutral density increases and (ii) occur in the coupled SW-M-I-T system in order to better understand how and where the heat sources -fueling upwellings and leading to localized neutral density increases- developed. By utilizing the innovative methodologies of interplanetary magnetic field (IMF) parameterization and flow channel (FC) classification, we were able to investigate various geophysical processes that had not been understood well and/or had been less investigated. The geophysical processes investigated occurred at various geomagnetic activity levels -ranging from moderate storms to superstorms- and sometimes were driven externally by solar-wind Alfven waves propagating away from the Sun.

Our efforts are documented in a series of journal articles published already (Horvath & Lovell, 2018a, 2018b, 2019a; 2019b) and currently are under review (Horvath & Lovell, 2020a; 2020b; 2020c) reporting new results and findings. These include the demonstrations of (1) significant energy deposition occurring deep in the polar cap along old-open magnetic field lines, (2) the antisunward propagating solar-wind Alfven waves' ability (a) to drive flux transfer events/flow channel events and to launch atmospheric gravity waves and (b) to infiltrate into the coupled M-I-T system where bouncing Alfven waves provided electromagnetic communications between the ionosphere and the plasma sheet and consequently rippled the plasma sheet's inner edge, (3) localized neutral density peak development within/over the less investigated and less understood eastward flow channel (E-FC) during high/low-latitude magnetopause reconnection events, (4) strong M-I-T coupling during storm-enhanced density (SED) events and plasmaspheric erosion events, (5) large sub-auroral polarization streams (SAPS) causing strong plasmaspheric erosions, and (6) SAPS flows' enhancement by large-scale travelling ionospheric disturbances (TIDs).

These new results and findings led to the unravelling of near-pole electromagnetic energy deposition via various types of FCs, ASAID development during magnetically quiet times, and large SAPS FC development under superstorm conditions. We highlight here also our first ASAID detection by utilizing Polar data and the first demonstrations of large-scale TIDs enhancing SAPS FCs and SAPS_WS (i.e. the structured version of SAPS).

These new results and findings contribute to the better understanding of many basic geophysical processes by explaining fundamental multiple inter-relationships and configurations. This improved understanding fills existing gaps in the community knowledgebase, adds directly to the ongoing sub-auroral and polar investigations carried out at the AFRL and to the MURI-IT project, and thus provides advancement in the field of space science.

Investigations carried out:

(1) Horvath, I., & Lovell, B. C. (2018a). Investigating high-latitude energy deposition events occurring during the 17 January 2005 geomagnetic storm. *Journal of Geophysical Research: Space Physics, 123(8),* 6760-6775. https://doi.org/10.1029/2018JA025465

Introduction:

It is well known that the accurate specification of high-latitude energy input by empirical models is important for reproducing thermospheric variations in a realistic way. With 5-6 August 2011 storm results, the studies of Huang et al. (2014a; 2014b) demonstrate that the current Weimer model not only misplaced the location of main energy input but also underestimated the total energy input. As revealed by the experimental Poynting flux ($S_{\parallel}$) values obtained from DMSP measurements, high $S_{\parallel}$ values were observed across the polar cap while enhanced $S_{\parallel}$ values appeared only in a marrow region of the auroral zone. Oppositely, the more recent study of Lu et al. (2016) demonstrates with results provided by the AMIE (Assimilative Mapping of Ionospheric Electrodynamics) procedure for the 17 January 2005 storm that there were two major energy deposition events (at 1200 UT and 1730 UT) and only 22-25% of the magnetospheric energy was dissipated in the polar cap, since most of the magnetospheric energy was deposited into the auroral zone.

Huang, C. Y., Y.-J. Su, E. K. Sutton, D. R. Weimer, and R. L. Davidson (2014a), Energy coupling during the August 2011 magnetic storm, *J. Geophys. Res. Space Physics*, 119, 1219–1232, https://doi:10.1002/2013JA019297.

Huang, Y., C. Y. Huang, Y.-J. Su, Y. Deng, and X. Fang (2014b), Ionization due to electron and proton precipitation during the August 2011 storm, *J. Geophys. Res. Space Physics*, 119, 3106–3116, doi:10.1002/2013JA019671.

Lu, G., A. D. Richmond, H. Lühr, and L. Paxton (2016), High-latitude energy input and its impact on the thermosphere, *J. Geophys. Res. Space Physics*, 121, 7108–7124, https://doi:10.1002/2015JA022294

Results:

In our study, we have investigated 17 January 2005 storm for the energy deposition events occurring deep in the polar cap region in order to unravel the underlying physical processes. We have investigated the relations among Poynting flux intensifications and flow channels (FCs) and localized neutral density increases plus the nature of the underlying reconnection events. Our observational results provide evidence that there had been significant energy depositions occurring deep in the polar cap (MLAT<78°) during the above described two major energy deposition events occurring at 1200 UT (see left panels of Figures 1.1-1.2) and 1730 UT (see right panels of Figures 1.1-1.2), and their associated Poynting flux increases occurred in flow channels above/within which the resultant localized neutral density increases developed.

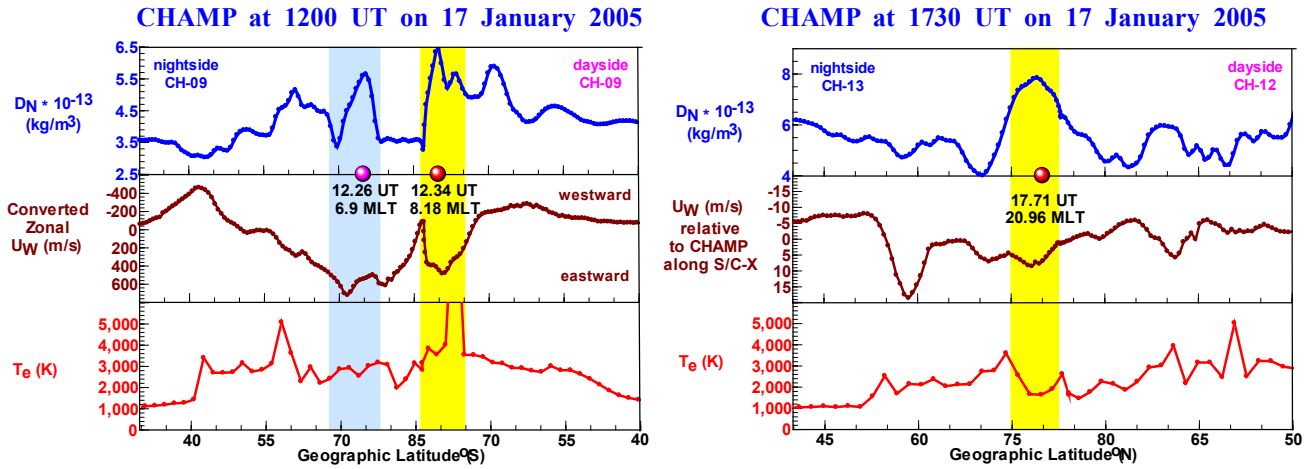

Figure 1.1: The multi-instrument CHAMP line plots illustrte the localized neutral density increases [see neural densit y (D_N) plots] develped plus the underlying flow channel signatures [see the zonal wind (U_W) plots] and enhanced electron temperatures (see Te plots).

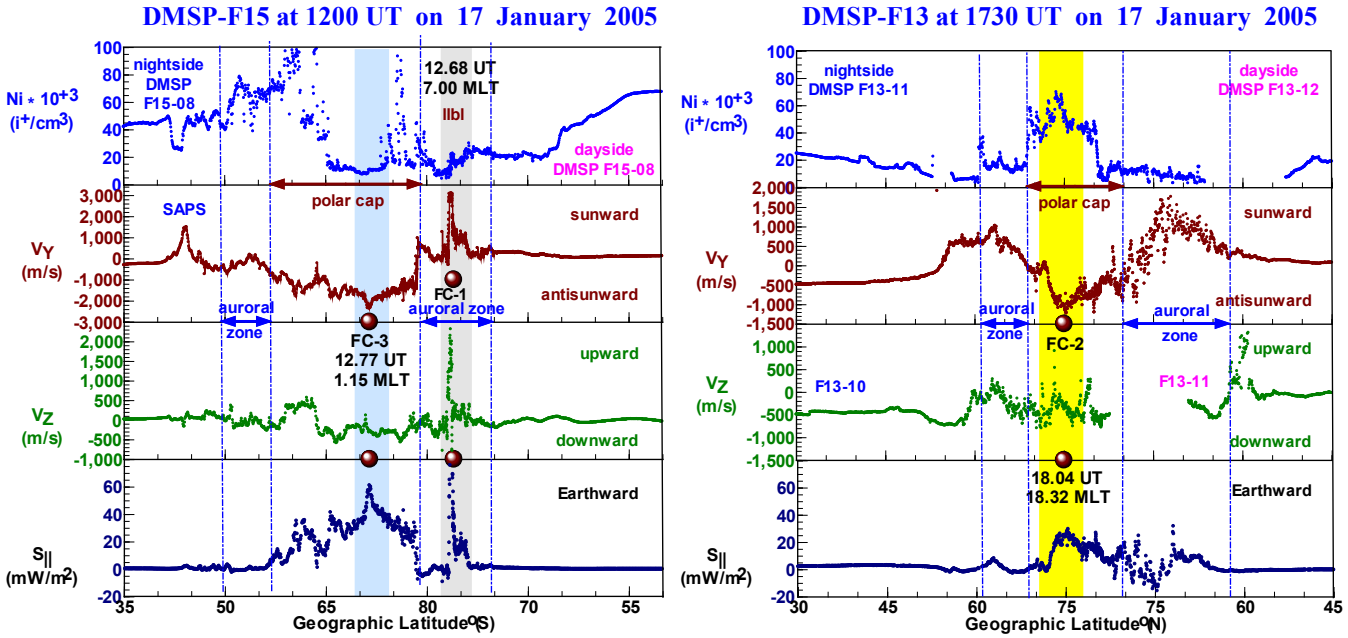

Figure 1.2: The matching DMSP passes tracked the same flow channels in the antisunward (or eastward) drift at local evening specified as a FC-3 type flow channel (left panel) and at daytime specified as a FC-2 type flow chan nel (right panel). The latitudinal Poynting flux ($S_{||}$) profiles reveal that Poynting flux (i.e. Joule heating) intensified in the entire polar cap region and locally maximized above/within these FC-3 and FC-2 types flow channels.

Conclusions:

From our observational results providing solid evidence we concluded that localized energy depositions into the central polar cap -via flow channels and during flux transfer events- played a major role in the development of the localized neutral density increases investigated during these this 17 January 2005 storm. These energy depositions occurred during the various types of reconnection events taking place along old-open field lines such as during dayside magnetopause reconnection (associated with FC-2), nightside magnetotail reconnection (associated with FC-3), and lobe reconnection (associated with FC-4). Thus, the AMIE generated Joule heating values did not provide a realistic representation of the energy deposition events occurring in the auroral and polar regions. Furthermore, atmospheric gravity waves (AGWs) played only a secondary role in the latitude distribution of the elevated neutral densities.

(2) Horvath, I., & Lovell, B. C. (2018b). Polar ion temperature variations during the 22 January 2012 magnetic storm. *Journal of Geophysical Research: Space Physics, 123(9),* 7806-7824. https://doi.org/10.1029/2018JA025727

Introduction:

Solar-wind Alfven waves transmitted across the bow shock generate pressure pulses in the magnetosheath, excite the magnetosphere, and therefore modulate SW-M-I-T coupling through pulsed magnetic reconnection events or flux transfer events (FTEs). The resultant ionospheric signatures of FTEs are called pulsed ionospheric flows (PIFs) appearing as enhanced convection flows or flow channels (FCs) during flow channel events (FCEs). Most of the incoming electromagnetic energy from the solar wind becomes deposited as earthward directed Poynting flux and drives magnetospheric convection and large-scale field-aligned currents (FACs). Earthward Poynting flux appears both as Joule heating and as particle precipitation in the ionosphere, and results in ion and neutral temperature enhancements in the coupled I-T system.

Recent studies investigate Joule heating responses to Poynting flux ($S_{||}$) inputs via monitoring ion temperature (Ti) and neutral density variations as a way of studying M-I-T coupling (Mishin et al., 2007; Huang et al., 2016, 2017). These studies focus on the dayside cusp and polar cap regions, and provide observational evidence revealing the significant amount of input energy received by the polar region along with the consequential I-T heating and neutral density perturbations appearing as localized polar cap neutral density increases. Their development can be explained with the process of solar wind energy deposition into the coupled M-I-T system as earthward Poynting flux via the dayside cusp or polar cap. Then, oppositely directed large-scale FACs connect within FCs, fuel Joule heating, and drive upwelling leading to the development of localized neutral density enhancements.

However, the observed different spatial distributions of $S_{||}$ and Ti maxima imply that there are spatial differences between the energy input (i.e. Poynting flux) and the resultant Joule heat (i.e. ion temperature) meaning that the spatial correlation of $S_{||}$ and Ti is not linear. But their underlying physical processes are not well understood. Such differences between $S_{||}$ and Ti maxima are recently reported (Huang et al., 2016) noting the 22 January 2012 storm as an example. In this study, our aim was to further investigate this magnetic storm in order to unravel the cause of such $S_{||}$ and Ti differences.

Huang, C. Y., Huang, Y., Su, Y.-J., Sutton, E. K. & Hairston, M. R. (2016). Ionosphere-thermosphere (IT) response to solar wind forcing during magnetic storms. *Journal of Space Weather and Space Climate*, 6, A4, https://doi:10.1051/swsc/2015041

Huang, C. Y., Huang, Y., Su, Y.-J., Huang, T., & Sutton, E. K. (2017). High latitude neutral mass density maxima. *Journal of Geophysical Research: Space Physics*, 122, 10,694–10,711. https://doi.org/10.1002/2017JA024334

Mishin, E. V., Marcos, F. A., Burke, W. J., Cooke, D. L., Roth, C., & Petrov, V. P. (2007). Prompt thermospheric response to the 6 November 2001 magnetic storm. *Journal of Geophysical Research*, 112, A05313. https://doi.org/10.1029/2006JA011783

Results:

Regarding the nature of this storm, our results reveal the pulsed nature of the 22-23 January 2012 storm (left panel of Figure 2.1) and the strong "Alfvenicity" of the solar wind due to the presence of antisunward propagating solar-wind Alfven waves (right panel of Figure 2.1). Evidence is provided by the episodic variations of interplanetary, geomagnetic, and ionospheric variables (left panel Figure 2.1) and by the one-to-one correlations between the respective components of solar wind velocity and interplanetary magnetic field (IMF) (see right panel Figure 2.1).

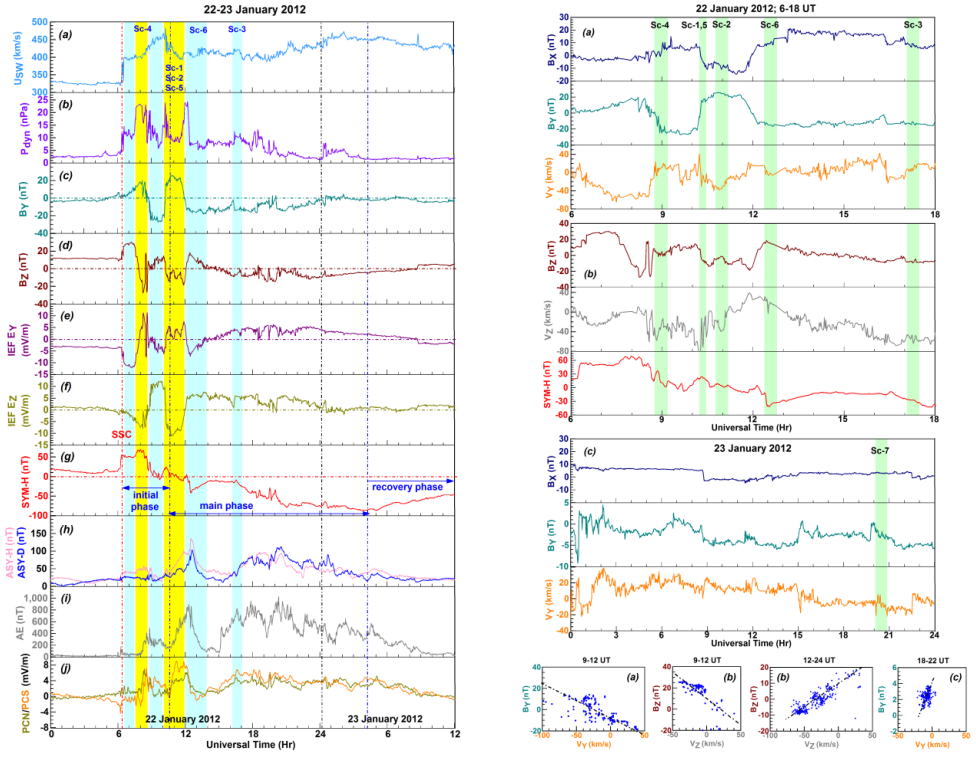

Figure 2.1 left panel: The 20 January 2012 storm evolution is depicted by the various time series and the shaded intervals indicate the pulsed nature of the storm and the scenarios investigated.
Figure 2.1 right panel: The time series of the corresponding IMF and solar wind components indicate the presence of solar-wind Alfven waves and their SYM-H signatures, while the scatter plots' negative gradients for $B_X<0$ and positive gradients for $B_X>0$ confirm the Alfven waves' antisunward propagation.

Regarding the thermospheric responses, our results reveal with various scenarios that:
(i) In Senario-1, the localized neutral density enhancement developed within/above a FC-2 where the charged and neutral particles moved differently suggesting the role of frictional heating in the confined Ti increase within/above this FC-2. Thus, the Ti intensification within this FC-2 had a strong Joule heating component as demonstrated by the direct correlation between the $S_{||}$ and Ti maxima at FC-2 latitudes, as shown in Figure 2.2.

(ii) In Scenario-2, the development of polar neutral density peak continued deep in the polar cap, close to the magnetic pole, and within/above a FC-1 wherein Ti locally decreased creating a Ti trough and thus demonstrating an inverse relationship between $S_{||}$ and Ti. This indicates that the dayside cusp had been stable for a while, possibly due to its quick response to the energy deposition received as $S_{||}$ (~70 mW/m^2) and thus implies a late stage of this FTE/FCE. Possibly, the neutrals had already responded to the high-speed ions, and therefore ions and neutrals travelled with the same speed ruling out frictional heating at FC-1 latitudes, as shown in Figure 2.3.

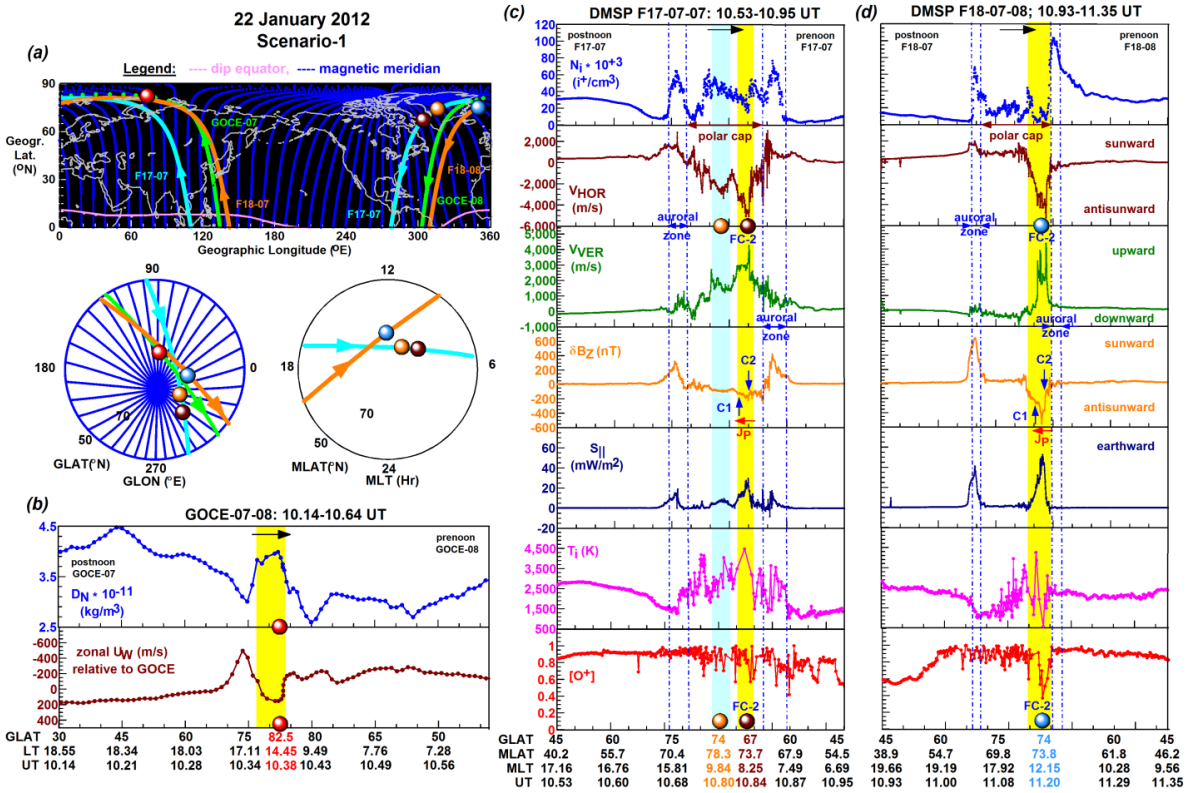

Figure 2.2: (a) The northern-hemisphere map and polar plots depict the satellite passes employed and the features of interest. (b) The GOCE line plot sets illustrate a neutral density increase in an eastward (or antisunward) zonal wind surge (indicated as shaded interval in yellow). (c) The matching DMSP line plot sets depict the underlying FC-2 (indicated as shaded interval in yellow) wherein the earthward Poynting flux ($S_{||}$) and ion temperature (Ti) increased and the fractional O^+ content decreased. The horizontal arrows indicate the travelling directions of GOCE and DMSP satellites.

Finally, we also documented with four scenarios (Sc-4—Sc-7) some Ti perturbations appearing in the polar cap as Ti oscillations during the storm recovery phase on 23 January (see Figure 2.4). As Scenario-7 shows, these Ti oscillations travelled across the polar region towards the equator and were driven by solar-wind Alfven waves. At that time, the polar cap region was small because of the poleward expansion of the auroral zone on both sides, due to the arrival of the westward travelling surge (WTS), which is the ionospheric signature of the substorm current wedge (SCW). But the formation of SCW is also associated with solar-wind Alfven waves bouncing back and forth between the two hemispheres and forming standing waves. In good agreement with this, the Ti perturbations shown in Scenario-7 originated from the postnoon auroral zone (shaded interval in yellow) and were supported by the Alfvenic solar wind fluctuations (shaded intervals in yellow, cyan, and gray).

Conclusions:

From these findings we concluded that during the FTEs and their resultant FCEs detected, there was a direct correlation between the earthward $S_{||}$ and the polar cap neutral density (D_N) increase occurring within/above the respective FC but the variation of Ti depended upon the stage of FTE/FCE development. We found a direct correlation among the variables of $S_{||}$, D_N, and Ti during the early stages of the FTEs/FCEs when the abruptly accelerated ions just met the slower responding neutrals and therefore there was still a large difference between their velocities enhancing frictional heating. Oppositely, Ti correlated inversely with the locally increased $S_{||}$ and D_N within/over the respective FC at the later stages of the FTEs/FCEs when the ions and neutrals moved already together reducing or ceasing frictional heating. Episodic vertical-velocity-correlated Ti oscillations further increased the complexity of Ti variations. These Ti oscillations were driven by antisunward propagating solar-wind Alfven waves, originated from polar FCs during FTEs/FCEs or from auroral eastward flow channels (E-FCs) indicating WTS/SCW during the poleward expansion of the auroral zone, and commonly propagated across the polar cap towards lower latitudes.

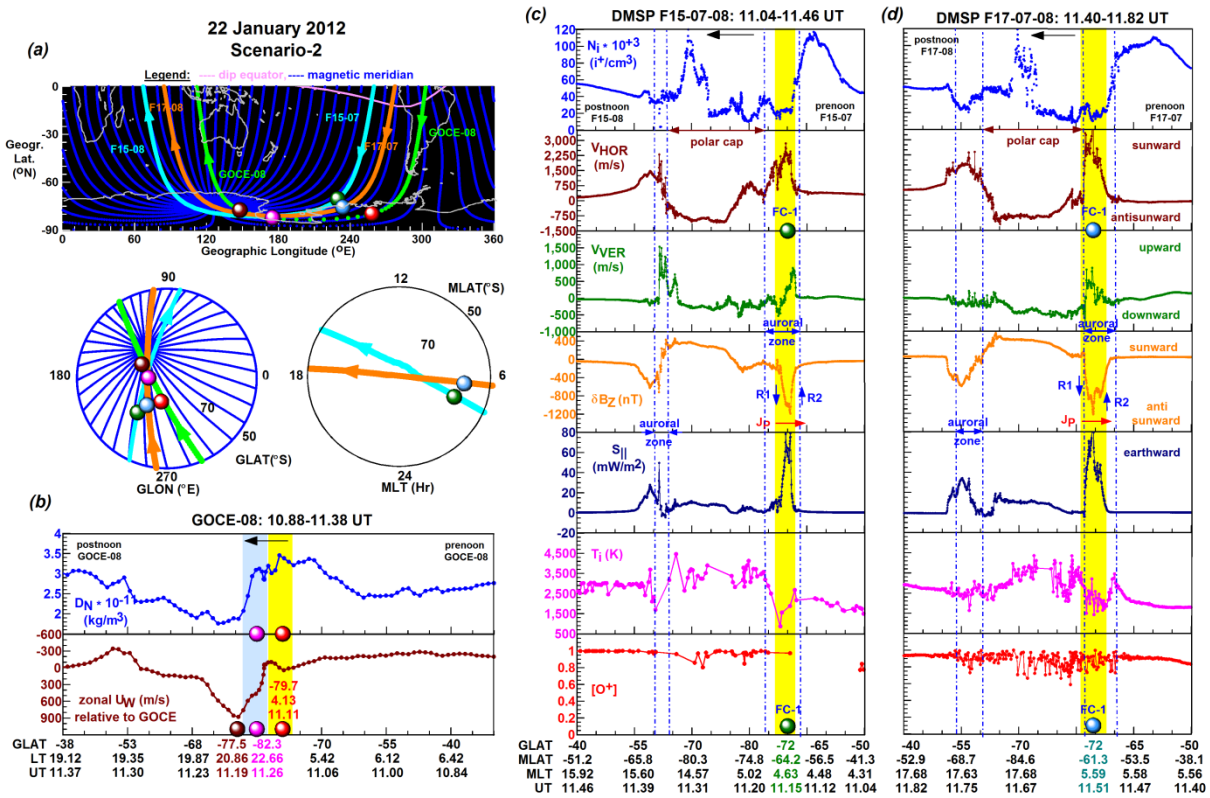

Figure 2.3: (a) The northern-hemisphere map and polar plots depict the satellite passes employed and the features of interest. (b) The GOCE line plot sets illustrate a neutral density increase in an eastward (or antisunward) zonal wind surge (indicated as shaded interval in yellow). (c) Each matching DMSP line plot sets depict a FC-1 (indicated as shaded interval in yellow) wherein the earthward Poynting flux ($S_{||}$) and ion temperature (Ti) increased and the fractional O^+ content decreased. The horizontal arrows indicate the travelling directions of GOCE and DMSP satellites.

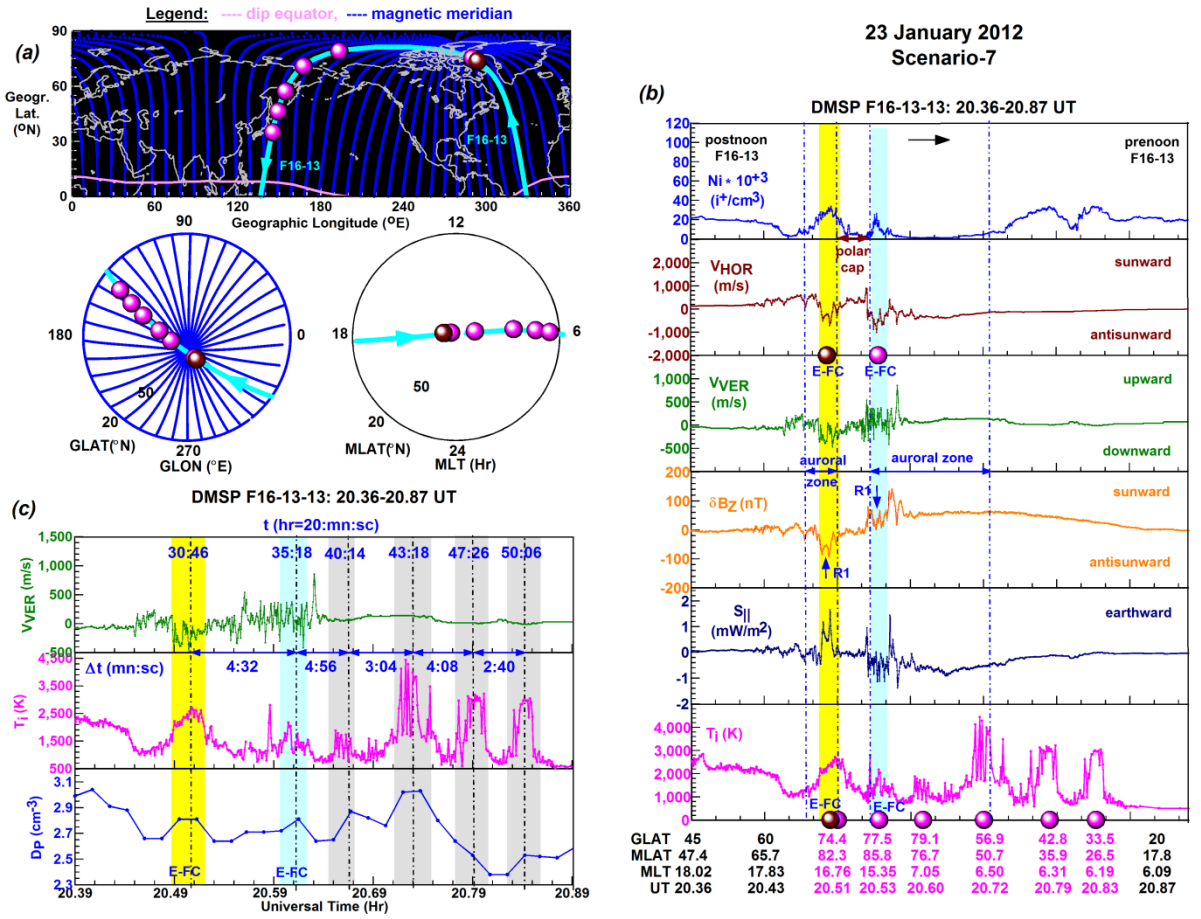

Figure 2.4: (a) The northern-hemisphere map and polar plots depict the DMSP satellite pass employed and the features of interest. (b) The DMSP polar cross sections depict the setting of episodic Ti variations, (c) the time series illustrate no correlation between the vertical drift and the Ti peaks in the absence of upwelling events, and the direct correlation of Ti peaks and solar-wind Alfven wave variations (see shaded intervals in yellow, cyan, and gray).

(3) Horvath, I., & Lovell, B. C. (2019a). Investigating the development of abnormal subauroral ion drift (ASAID) and abnormal subauroral polarization stream (ASAPS) during the magnetically quiet times of October 2003. *Journal of Geophysical Research: Space Physics*, *124(1)*, 715-733. https://doi.org/10.1029/2018JA026230

Introduction:

Appearing as inverted subauroral ion drifts (SAID) or inverted sub-auroral polarization streams (SAPS) during magnetically disturbed and quiet times, the abnormal SAID (ASAID) or abnormal SAPS (ASAPS) are recently discovered phenomena (Voiculescu and Roth, 2008). While disturbed-time ASAID/ASAPS development can be explained with the formation of a plasmaspheric shoulder structure creating a magnetospheric cold-plasma-shoulder—hot-ring-current interface layer (Voiculescu, 2012; Horvath and Lovell, 2018), this study has revealed that the quiet-time ASAID/ASAPS development must be due to another process since the plasmaspheric shoulder structure cannot develop during prolonged quiet times. Therefore, another process must be operational during continuing quiet times leading to the development of a certain magnetospheric cold plasma structure, whose combination with the hot ring current layer triggers the development of a quiet-time ASAID/ASAPS. Our main aims were to find out (1) how the quiet-time magnetospheric cold plasma structure appeared and became created, and (2) how the quiet-time ASAID/ASAPS feature developed. We speculated that (i) this quiet-time process could be driven by antisunward solar-wind Alfven waves and bouncing Alfven waves, and (ii) this certain magnetospheric cold plasma structure could be generated by bouncing Alfven waves (iii) triggering plasma sheet rippling, as shown in the study of Maynard et al (1996) as shown in the top left penal of Figure 5 and thus (iv) leading to the development of a magnetospheric cold-plasma-ripple—hot-ring-current interface. Various observational results and six scenarios (Sc-1—Sc-6) provide observational evidence.

Horvath, I., & Lovell, B. C. (2018). Investigating the development of abnormal subauroral ion drift (ASAID) and abnormal subauroral polarization stream (ASAPS) during the magnetically active times of September 2003. *Journal of Geophysical Research: Space Physics*,123, 1566–1582. https://doi.org/10.1002/2017JA024870

Maynard, N.C., Burke, W.J., Basinska, E.M., Erickson, G.M., Hughes, W.J., Singer, H.J., Yahnin, A.G., Hardy, D.A., & Mozer, F.S. (1996). Dynamics of the inner magnetosphere near times of substorm onsets. *J. Geophys. Res.*, 101(A4), 7705–7736. doi:10.1029/95JA03856

Voiculescu, M. (2012). Ionospheric perturbations induced by interplanetary and solar forcing. International Conference SOLAR AND HELIOSPERIC INFLUENCES ON THE GEOSPACE, Bucharest, ROMANIA, 1 – 5 October 2012. URL:www.geodin.ro/CONFERENCE2012/.../Iono_perturb_solar_mag_forcing_tosend.pdf

Voiculescu, M. & Roth, M. (2008). Eastward sub-auroral ion drifts or ASAID. *Ann. Geophys.*, 26, 1955-1963, https://doi.org/10.5194/angeo-26-1955-2008.

Results:

Our investigation covering the 9-12 October 2003 magnetically quiet period with four scenarios (Sc-1—Sc-4) has revealed and demonstrated with observational results some of the significant aspects of the geophysical conditions underlying the development of these quiet-time ASAID/ASAPS features. We have shown the continuous presence of antisunward solar-wind Alfven waves during the detection of ASAID/ASAPS by DMSP F15 (see Figures 3.1a-d in right panel) and the Interplanetary E field (IEF) E_Y and E_Z components appearing with similar amplitudes that are oppositely directed (see Figure 3.1e in right panel). These IEF observations imply some favorable conditions, created for solar-wind Alfven waves—magnetopause coupling, that led to dayside magnetopause and nightside magnetotail reconnection events as the Dungey convection cycle unfolded (see bottom left panel of Figure 3.1). Bouncing Alfven waves are indicated by the rapid fluctuations of the IEF E_Y and E_Z components (see Figure 3.1e in right panel) and thus imply plasma sheet rippling.

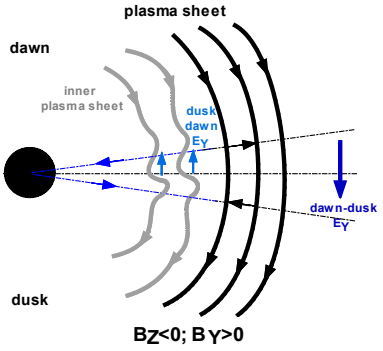

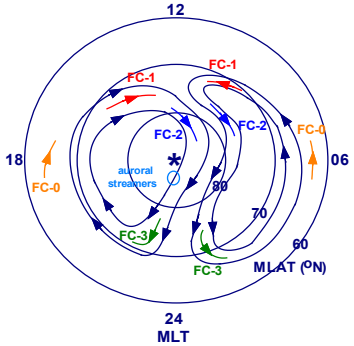

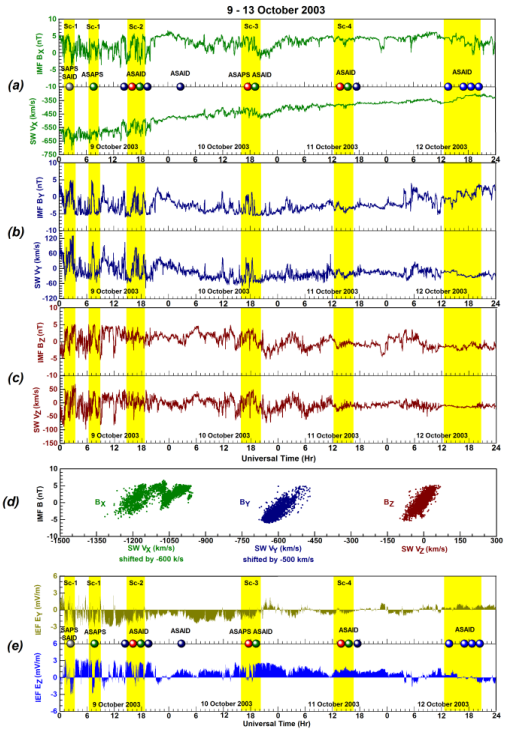

Figure 3.1 top left panel: Modified after Figure 12b of Maynard et al (1996), the diagram illustrates the rippled inner edge (in gray) of the plasma sheet, as the dusk-dawn directed cross-tail E_Y (in blue) works against the dawn-dusk directed convection E_Y (in black). Figure 3.1 bottom left panel: The FC types of FC-0 (enhanced auroral return flows), FC-1 (dayside reconnection on newly-open field lines), FC-2 (dayside reconnection on old-open field lines), FC-3 (nightside reconnection closing old-open field lines), and auroral streamers evidencing magnetotail reconnection related earthward plasma flows are shown. Figure 3.1 right panel: the time series constructed with the (a) X, (b) Y, and (c) Z components of the IMF and solar wind (SW) data illustrate the presence of solar-wind Alfven waves (shaded intervals). (d) The scatter plots constructed for these IMF-SW components depict their positive linear correlations characteristics of solar-wind Alfven waves. (e) The time series illustrate the variations of the IEF EY and EZ components. Their opposite phase is evident during the ASAID/ASAPS events (shaded intervals).

Our Scenario-1 shown in Figure 3.2 demonstrates that the periodic variation of IEF E_Y triggered SAPS-SAID development during its dawn-dusk polarity (implying undershielding) and ASAPS development during its dusk-dawn orientation (implying overshielding), while sunward wind surges intensified and particle injections occurred.

Our Scenario-2 shown in Figure 3.3 provides observational evidence of strong ASAID development during the dusk-dawn orientation of the IEF E_Y. During that time, the dayside magnetopause and nightside magnetotail reconnection events were driven externally by these antisunward propagating solar-wind Alfven waves and associated solar wind surges. Evidence is provided by the ionospheric flow channel signatures specified as FC-1 wherein region 1 (R1) and R2 FACs connected (R1-R2 FACs) during dayside magnetopause reconnection and as FC-3 wherein cusp (C1-C2 FACs) currents connected during nightside magnetotail reconnection. Thus, these ASAID features developed during the process of magnetotail reconnection, when the cold high-density plasma sheet had been building up in the distant tail (~25 R_E) region and becoming delivered into the near-Earth region to geosynchronous orbit (6.6 R_E), as detected by the LANL satellite.

Conclusions:

From these observational results we concluded that (1) the antisunward solar-wind Alfven waves propagated through the dayside and nightside reconnection regions into the coupled M-I system where they bounced back and forth, and these bouncing Alfven waves drove impulsive cross-tail E_Y variations, which, in turn, rippled the plasma sheet's inner edge. (2) This plasma sheet rippling led to the formation of a magnetospheric cold-plasma-ripple—hot-ring-current interface layer, which possibly developed in a turbulent plasmaspheric boundary layer, and generated an earthward (or inward) magnetospheric E field. (3) As mapped down to the ionosphere along the magnetic field lines, an ionospheric cold-plasma-trough—hot-ring-current interface layer and a southward (or equatorward) ionization E field formed, where the southward (or equatorward) ionization E field drove the plasma antisunward (or eastward) in the sub-auroral flow channel forming an ASAID/ASAPS feature.

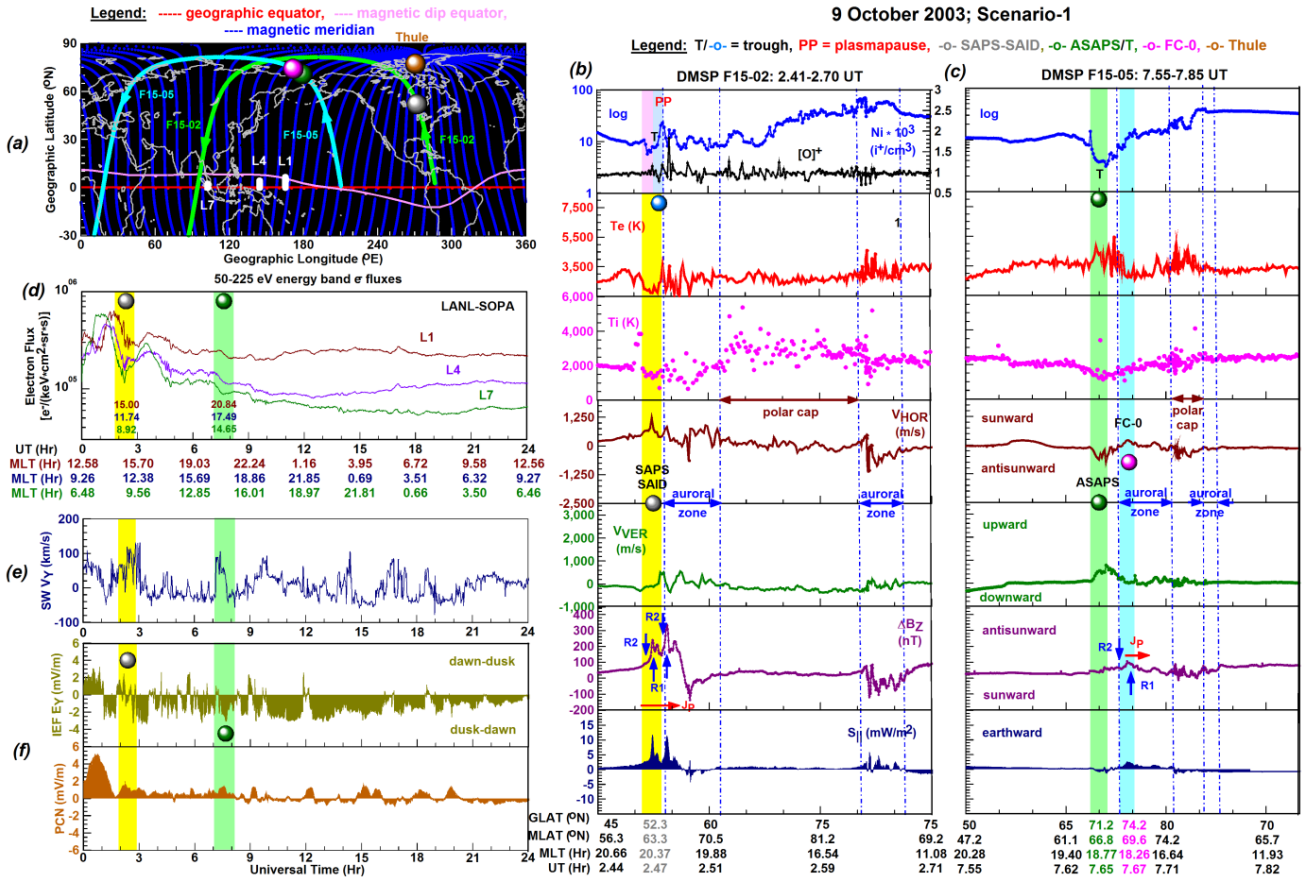

Figure 3.2: Scenario-1's (a) the northern-hemisphere map depicts the DMSP F15-02 (green) and F15-05 (cyan) passes tracking the features of interest. (b)-(c) The DMSP F15 polar cross-sections depict a combined SAPS-SAID feature (shaded interval in yellow) and an ASAPS feature (shaded interval in green), and an FC-0 (shaded interval in cyan). These polar cross-sections are constructed with ion density (Ni), electron temperature (Te) and ion temperature (Ti), zonal (V_{HOR}) and vertical drift (V_{VER}), and cross-track magnetic deflection component (ΔB_Z) data and the computed Poynting flux ($S_{||}$) values. J_P indicates Pedersen currents and the large-scale FACs include R1 and R2 currents. (d) The time series of high-energy electron fluxes measured by LANL SOPA illustrate electron flux increases. (e) The time series solar wind V_Y component illustrates the solar wind surges occurring during the SAPS-SAID and ASAPS events (shaded intervals). (f) The time series of IEF E_Y and PCN index show solar-wind Alfven wave-driven variations during these SAPS-SAID and ASAPS events (shaded intervals).

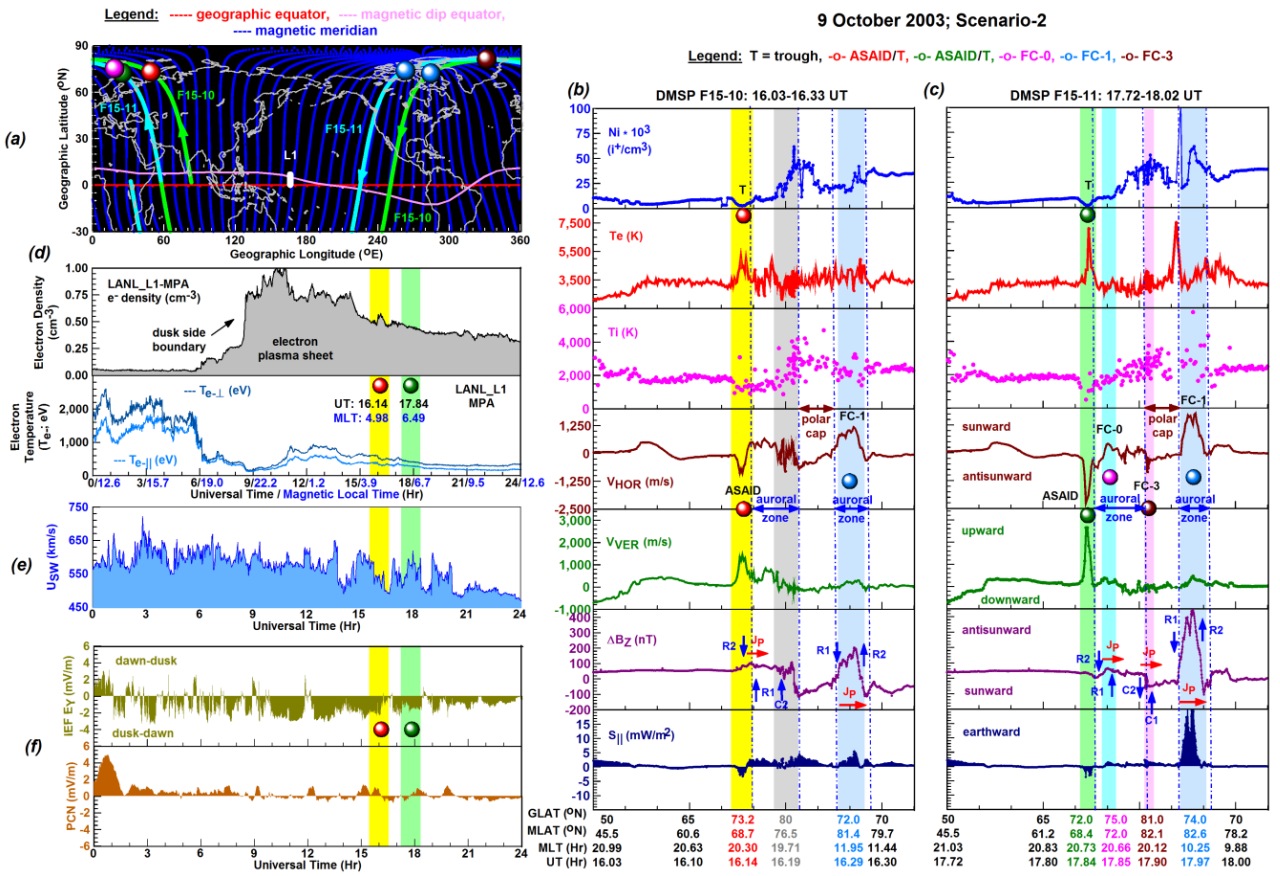

Figure 3.3: Similar to Figure 3.2 but for Scenario-2 depicting two ASAID features (shaded intervals in yellow and green), a FC-0 (shaded interval in cyan), two FC-1s (shaded intervals in blue), a FC-3 (shaded interval in magenta), and auroral streamers (shaded interval in gray). (d) The LANL MPA high-energy electron density and temperature measurement detected the electron plasma sheet in the night-time MLT sector. (e) The solar wind flow speed measurements tracked the signatures of solar wind surges during these ASAID events (shaded intervals). (f) The time series of IEF E_Y and PCN index imply the presence of dusk-dawn directed cross-tail E_Y and overshielding conditions and solar-wind Alfven wave driven variations during these ASAID events (shaded intervals).

(4) Horvath, I., & Lovell, B. C. (2019b). Abnormal sub-auroral ion drifts (ASAID) and Pi2 pulsations observed by the Polar satellite during the magnetically quiet times of October 2003. *Journal of Geophysical Research: Space Physics, 124(7)*, 6097-6116. https://doi.org/10.1029/2019JA026725

Introduction:

In the night-time sector, low-latitude Pi2 pulsations (40-150 s) appear as transient features and are associated with substorm expansion phase onsets, and can also be directly driven (i.e. without any MHD resonances or Alfvenic standing waves) by earthward bursty bulk flows (BBFs) that are the signatures of the major transports of mass, energy, and magnetic flux in the plasma sheet. Geosynchronous spacecraft measured magnetospheric and plasmaspheric magnetic (B) field and electric (E) field data permit the detailed investigations of Pi2s and their mode structures. Such measurements made by the Polar satellite are particularly useful since they provide 3-dimensional (3-D) B field and E field values. The combination of 3-D E field data and plasma density measurements also allows the simultaneous detections of the SAID/SAPS feature's radially outward E_Z component and the nearby plasmapause (Mishin et al., 2010; Kim et al., 2010; Mishin, 2013). However, such observations demonstrating the radially inward (or earthward) orientation of the ASAID/ASAPS E field are still undocumented.

In this study, we continued our quiet-time ASAID/ASAPS investigations by utilizing Polar satellite data covering the magnetically quiet time period of 9-12 October 2003. Our main aims are (1) to provide observational evidence of ASAID development in the close vicinity of the plasmapause and its earthward directed radial E field, (2) to demonstrate the presence of Pi2 pulsations/bouncing Alfven waves and their significance in driving E field variations during the development of ASAID, and (3) to investigate the role of nightside magnetotail reconnection in ASAID development.

Kim, K.-H., Mozer, F. S., Lee, D.-H., & Jin, H. (2010). Large electric field at the nightside plasmapause observed by the Polar spacecraft. *J. Geophys. Res.*, 115, A07219, https://doi:10.1029/2010JA015439

Mishin, E. (2013). Interaction of substorm injections with the subauroral geospace: 1. Multispacecraft observations of SAID. *J. Geophys. Res. Space Physics*, 118, 5782–5796. https://doi:10.1002/jgra.50548

Mishin, E. V., Puhl-Quinn, P. A., & Santolik, O. (2010). SAID: A turbulent plasmaspheric boundary layer *Geophys. Res. Lett.*, 37, L07106. https://doi:10.1029/2010GL042929

Results:

By utilizing closely correlated multi-instrument Polar and DMSP F15 passes, we demonstrated the detections of two ASAID features over the Northern Hemisphere on 10 October 2003 (see left panel of Figure 4.1). These detections were

made by Polar at 3.8 UT (dot in red) and by DMSP F15 at 3.97 UT (dot in purple). Thus, the two satellites possibly tracked the same ASAID flow channel. While the Polar E_{XY} and E_Z line plots tracked the ASAID feature's antisunward and earthward E field components, the F15 V_{HOR} line plot detected its antisunward plasma drifts. Although there were no Polar spectrogram images of ions and electrons available, we could specify the regions of plasmasphere and plasma sheet from the Polar electron density (Ne) and plasma density (Np) values, as they are quite different within the plasmasphere (see shaded interval in yellow in left panel of Figure 4.1) but similar within the plasma sheet (see shaded interval in blue in left panel of Figure 4.1). Both Polar and F15 detected the cold Ti region in the vicinity of the plasmapause (PP) that is a significant feature attributed to the development of the ionospheric cold-plasma-trough—hot-ring-current interface. Furthermore, the periodic pulsations are also seen in the various Polar E and B field measurements and also detected by DMSP F15 in the postnoon auroral zone. As the filtered Polar B_Y line plot shows, such periodic pulsations created a positive amplitude at ASAID latitudes (shaded interval in yellow) and a steep B field gradient at the PP where ASAID peaked.

We have also investigated the larger region of the PP and ASAID (see bottom right Figure 4.1) in order to observe how the Pi2 pulsations/plasma sheet rippling appeared in the vicinity of the PP/ASAID. Such investigation was possible for this ASAID event, since Polar tracked the outer edge of the plasmasphere at $L \approx 8\ R_E$ that is a common value for magnetically quiet times. Both the filtered B_Y component and the direct observations of ion drift V_X and V_Y components depict largely enhanced localized oscillations near the PP (shaded interval in yellow). Since only the filtered B_Y component displayed the strongest B field oscillations (in the azimuthal direction), these are toroidal mode oscillations. Such enhanced and highly localized toroidal wave amplitudes appearing near the PP imply the localized increase of Alfven wave energy and are typical for field line resonances (FLRs) when the coupling between the cavity-mode eigenfrequency and the field line eigenfrequency is most efficient and when the fast-mode waves and the shear Alfven waves couple. Meanwhile, the transverse perturbation (ΔB_T) component increased to ~5.75 nT within the PP region (shaded interval in yellow) and thus implies the dramatic increase of large-scale FACs acting as a possible driver of these enhanced wave amplitudes. Thus, this ΔB_T increase was due to the diversion of cross-tail currents into the large-scale R1 and R2 FACs that connect through the ionosphere. But the compressional (δB_C) perturbation component increased only to a small value of ~0.75 nT indicating that the compressional plasma pressure buildup was small at PP latitudes.

An interesting feature of Polar Event 1 is the detections of $E_{P\text{-}P}$, E_{XY} and E_Z burst and multiple PP crossings in the rippled outer plasmasphere (top left and right panels of Figure 4.2). We specified these E field bursts as the manifestations of two ASAID features (when E_{XY} was antisunward and E_Z was earthward) and a SAID feature (when both E_{XY} and E_Z were sunward directed). These Polar detections are consistent with the alternating DMSP F15 detections of SAID and ASAID, shown in our previous described above study and here in bottom left panel of Figure 4.2), that were made by individual DMSP F15 detections during two consecutive F15 passes. Although Polar detected SAID features are reported by many previous studies (see details in section 1), this study is the first to demonstrate multiple ASAID detections and mixed ASAID and SAID detections that are commonly related to multiple PP crossings.

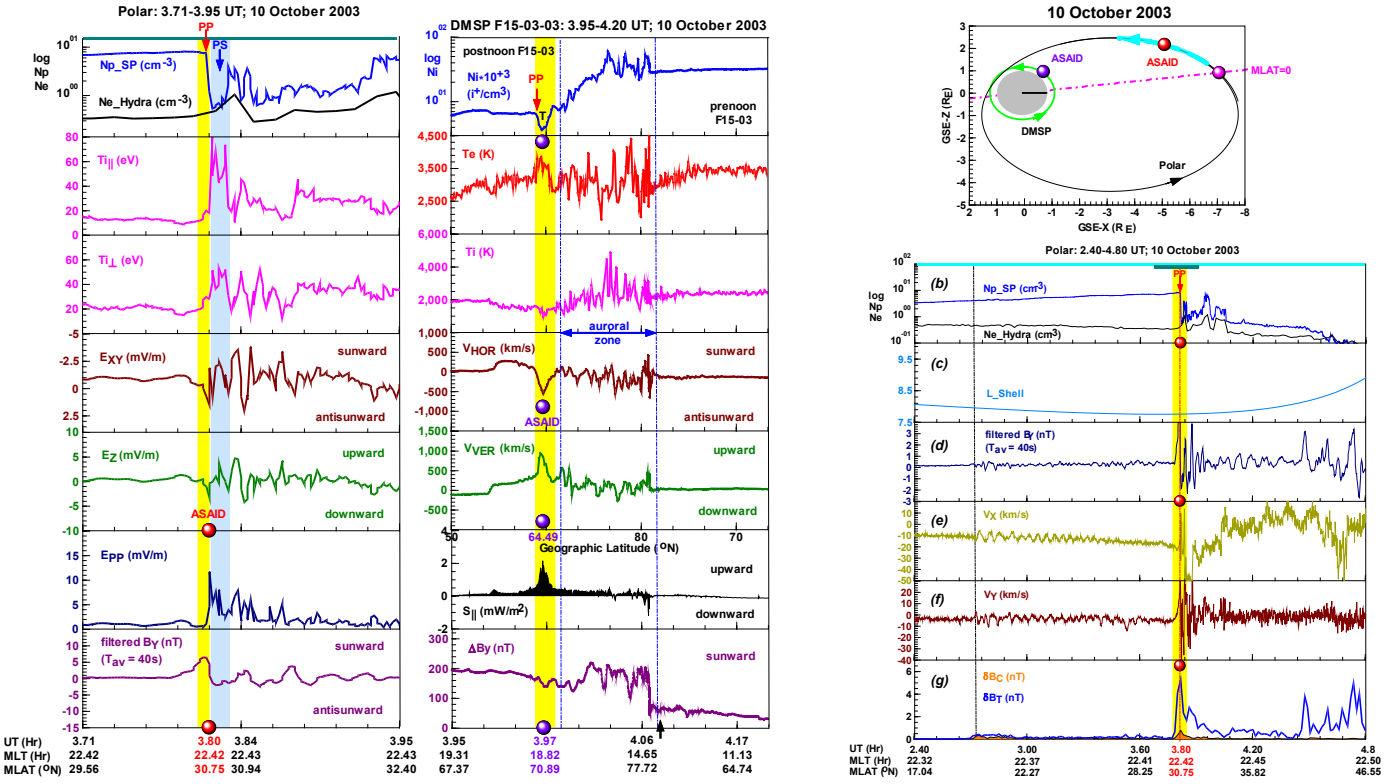

Figure 4.1 (left panel) The Polar and DMSP line plot sets depict the plasma environments of the ASAID features detected on 10 October 2003. (top right panel) The GSE-X vs GSE-Z plot illustrates the orbits of Polar and DMSP F15 on 10 October 2003 with their respective ASAID detections. The Polar orbit section of our interest in indicated in cyan and the crossing of GSM-Z=0 (in magenta) by Polar on the nightside is indicated by symbol dot in magenta. (bottom right panel) A larger section (cyan) of the coinciding PP/ASAID illustrates the locally enhanced amplitude of periodic pulsations (shaded interval in yellow) seen in the filtered B_Y data and in the ion drift data (V_X; V_Y) where the transverse perturbation (ΔB_T) component increased dramatically to ~5.75 nT but the compressional (δB_C) perturbation component remained low (~0.75 nT).

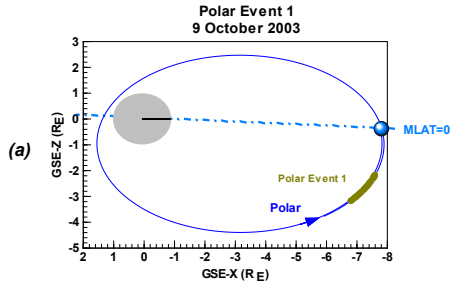

Figure 4.2 top left panel: The GSE-X vs GSE-Z plot illustrates the orbit of Polar satellite, Polar Event 1 and the Polar satellite's nightside magnetic equator (MLAT=0) crossing point (dot in light blue).

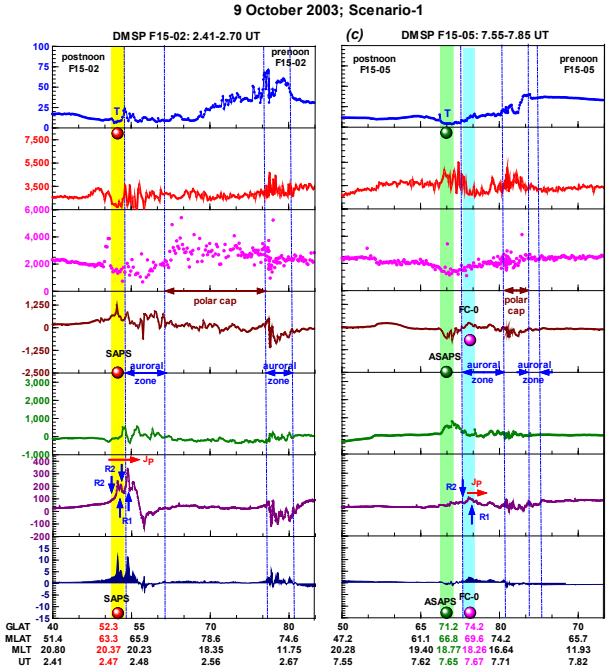

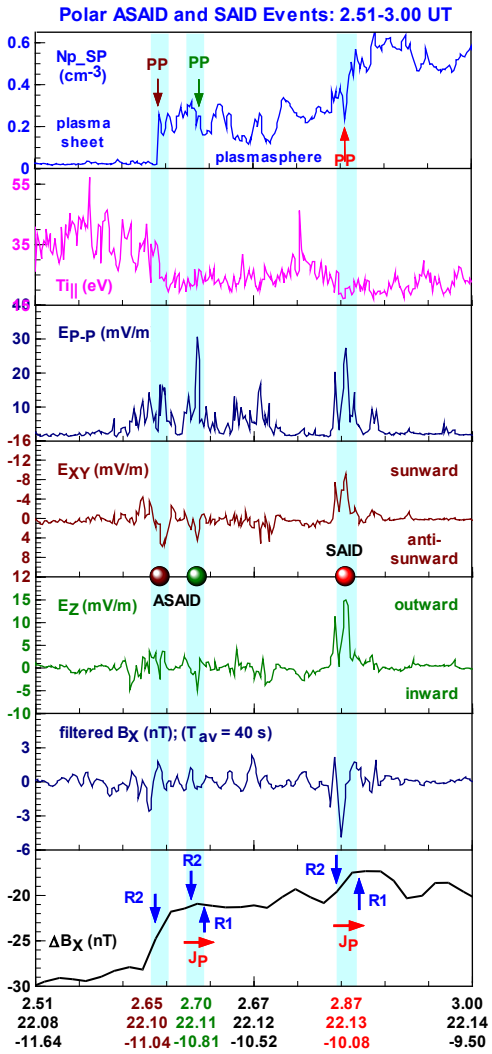

Figure 4.2 right panel: A detailed presentation depicts multiple PP crossings (PP in dark red, green, red) is constructed with plasma density (Np), field aligned ion temperature ($Ti_{||}$), E field components (E_{P-P}; E_{XY}; E_Z, filtered B_X and deflection component (ΔB_X). Then, two ASAID features (dots in dark red and green) and a SAID feature (dot in red) were detected (shaded intervals in light cyan).

Figure 4.2 bottom left panel: The DMSP F15 polar cross-sections depict consistent SAPS (shaded interval in yellow) and ASAPS (shaded interval in green) features.

Conclusions:

From these observational results obtained we conclude that the quiet-time ASAID/ASAPS formation investigated, occurring during a series of substorms and also in the absence of any substorm activity, was due to the continuous presence of solar-wind Alfven waves, and the localized increase of Alfven wave energy, manifested as FLRs. Solar-wind Alfven waves drove externally a series of magnetopause-magnetotail reconnections leading to the continuous rippling of the plasma sheet's inner edge and the plasmasphere's outer edge via a series of cross-tail current disruptions. These disruptions' tailward and earthward propagations were tracked by Cluster_C2 and Polar respectively along with their common feature, which is the convection flows' local reversal by the dawnward cross-tail E_Y causing plasma rippling by reversing the convection flows. Finally, we note here that this study's Polar observations provide observational evidence for the first time and thus verify that the ASAID related E_Z is earthward directed. Furthermore, this study demonstrates also for the first time multiple PP crossings and multiple ASAID-dawnward E_Y and SAID-duskward E_Y detections in the plasmasphere's rippled outer edge with multi-instrument Polar observations.

(5) Horvath, I., & Lovell, B. C. (2020a). Investigating Magnetosphere-Ionosphere-Thermosphere (M-I-T) coupling occurring during the 7-8 November 2004 Superstorm. *Journal of Geophysical Research: Space Physics* (accepted on 5 February 2020)

Introduction:

Magnetic reconnection is a process that facilitates the interconnection of interplanetary magnetic field (IMF) and geomagnetic field and thus allows the transfer of mass/energy/momentum from the Earth's magnetosheath to the magnetosphere (M) and then to the ionosphere (I) and thermosphere (T) creating a coupled M-I-T system. Reconnection with a time-varying nature produces a series of flux transfer events (FTEs; Russell & Elphic, 1978). As the magnetosphere couples with the ionosphere, the FTE's ionospheric signatures appear at ionospheric altitudes as auroral events, plasma convections and flow channels (FCs), and large-scale field aligned currents (FACs).

Via M-I-T coupling, the transferred mass/energy/momentum to the thermosphere leads to Joule and electron heating generating storm-time equatorward directed thermospheric wind surges, which, in turn, drive both neutral gas upwellings and composition changes. These changes can be parameterized and quantified by the O/N_2 ratio of which decrease or increase causes ionospheric depletions or enhancements respectively and of which changes can be redistributed by horizontal neutral

winds and molecular redistribution latter on (Kil et al., 2011) and by the NO content of which overproduction, caused by low-energy (<1keV) particle precipitations, results in reduced thermospheric uplift and density increase due to cooling (Knipp et al. 2013; 2017). But these storm time thermospheric wind surges and resultant composition changes are unlikely to cause large ionospheric plasma density depletions on their own (Clilverd et al., 2000). The combination of strong convection and SAPS E fields is needed to erode the dusk sector plasmasphere (Foster et al., 2005). Therefore, in order to understand the coupled M-I-T system, it is significant to understand how the coupling occurs between the magnetosphere and ionosphere and how the thermosphere couples with the coupled M-I system.

In this study, the main focus was on M-I-T coupling occurring during the 7-8 November 2004 Superstorm. We investigated how the magnetosphere coupled with the ionosphere and then to the thermosphere in order to better understand the underlying physical mechanisms. We also analyzed the relations of flux transfer events (FTEs) to the localized neutral density increases by investigating the development of these increases within/over their respective flow channels (FCs), since FCs are the ionospheric signatures of FTEs, and by specifying the FC types. We also investigated the development of localized neutral density increases during storm-enhanced density (SED) events and during plasmaspheric erosion events.

Clilverd, M. A., Jenkins, B., & Thomson, N. R. (2000). Plasmaspheric storm time erosion. *Journal of Geophysical Research*, *105(A6)*, 12,997– 13,008. https://doi:10.1029/1999JA900497

Foster, J. C., Coster, A. J., Erickson, P. J., Holt, J. M., Lind, F. D., Rideout, W., McCready, M., van Eyken, A., Barnes, R. J., Greenwald, R. A., & Rich, F. J. (2005). Multiradar observations of the polar tongue of ionization. *Journal of Geophysical Research, 110*, A09S31.https://doi:10.1029/2004JA010928.

Kil, H., Kwak, Y.-S., Paxton, L. J., Meier, R. R., & Zhang, Y. (2011). O and N_2 disturbances in the F region during the 20 November 2003 storm seen from TIMED/GUVI, *Journal of Geophysical Research*, *116*, A02314. https://doi:10.1029/2010JA016227

Russell, C. T., & Elphic, R. C. (1978). Initial ISEE magnetometer results: Magnetopause observations. *Space Science Reviews*, *22(6)*, 681–715. https://doi.org/10.1007/BF00212619

Results:

Our scenarios demonstrate strong M-I-T coupling when the localized neutral density enhancements developed during (i) FTEs unfolding during X_L reconnection and (ii) within/over FC-1 and FC-2 associated with auroral arcs or poleward moving auroral forms (PMAFs). While the storm-time sub-auroral polarization streams (SAPS) electric (E) field drove the storm-enhanced density (SED) plume plasma poleward and sunward across the polar cap, the neutral density also increased within or at the edge of the polar cap. Thus, a strong I-T coupling was displayed by the simultaneously increased neutral density, electron density, and electron temperature demonstrating that Joule heating, powered by small-scale-FACs, fueled upwelling leading to localized increases both in neutral density and in electron density.

Here, in Figure 5.1 we show the FTEs (middle panel) detected by Cluster_C1 during Event 2 (left panel) when the DMSP F15 detected a FC-2 (dot in blue) and CHAMP detected a neutral density peak (dot in cyan) as the polar plot illustrates (right panel).

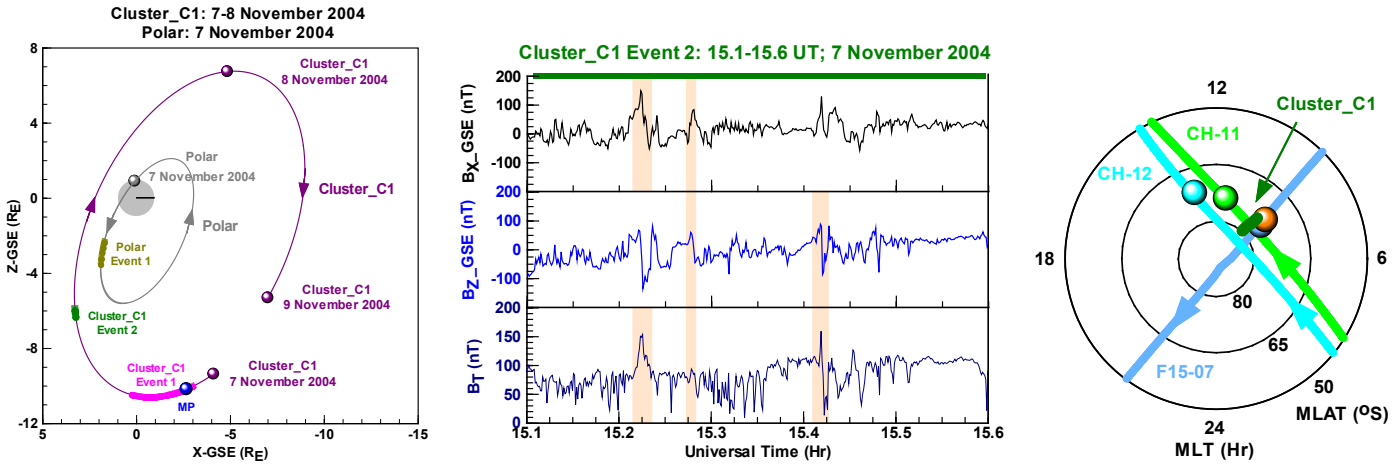

Figure 5.1: During Event-2 (right panel), the Cluster_C1 satellite detected a series of flux transfer events (FTEs) as indicated by the +/- B field rotations and enhanced total B field (B_T; shaded intervals; middle panel). FTE signature at the footprint of Cluster C1 (dark green) is closely correlated with the FTE signature of FC-2 detected in the ionosphere (dot in blue) and thermosphere (dot in cyan; right panel).

In Figure 5.2, we show this strong M-I-T coupling occurring during low-latitude X_L magnetopause reconnection when the localized neutral density increase occurred within/over a FC-2 and at the edge of the storm-enhanced density (SED) plume plasma increasing electron densities.

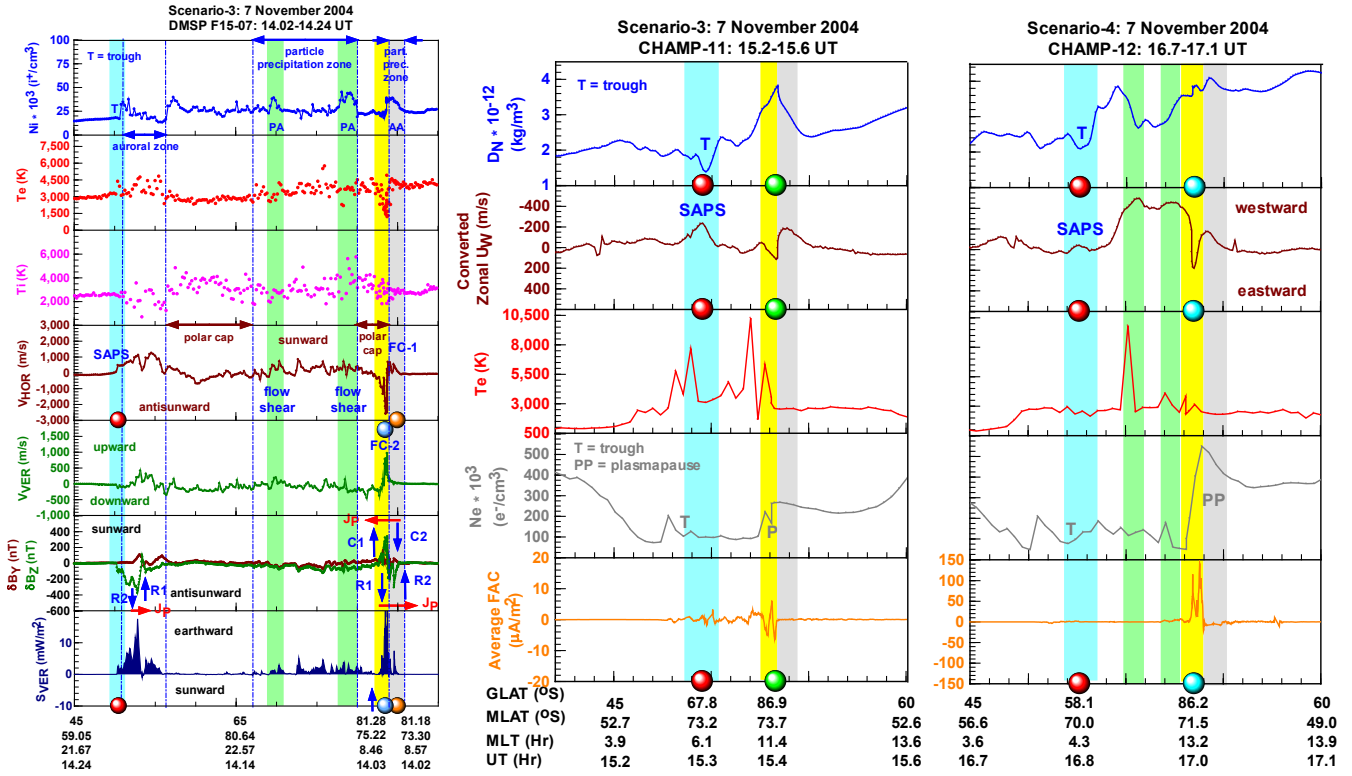

Figure 5.2: The DMSP F15 (left panel) and CHAMP (middle and right panels) scenarios illustrate strong M-I-T coupling with the enhanced electron and neutral densities, electron temperature, and small-scale FACs appearing within/above a FC-2 that is a signature of FTE.

As our scenarios demonstrate, the development of localized neutral density increases continued during dayside high-latitude X_H reconnection and within/over FC-4 associated with polar arcs and during plasmaspheric erosion events driven by the strong storm-time SAPS E fields. Then, the neutral density increases developed due to the quite intense earthward electromagnetic energy deposition (~170 mW/m^2 in Sc-7) within their respective FC-4s implying strong M-I-T coupling as the magnetosphere became preconditioned by the strong storm-time SAPS E field that swept the SED plume plasma to the ionospheric dayside cusp and magnetospheric dayside merging region. But the low electron density (created by plasmaspheric erosion), high neutral density, mid electron temperature, and weak small-scale FACs seemingly suggest weak I-T coupling.

Here, in Figure 5.3, we show the matching CHAMP Scenario-5 and DMSP F15 Scenario-7, which depict the development of localized neutral density peak within/above FC-4 occurring during a high-latitude X_H reconnection event and implying strong M-I-T coupling. But this event occurred during plasmaspheric erosion. Thus, the localized neutral density peak developed in the eroded polar cap region seemingly indicating weak I-T coupling

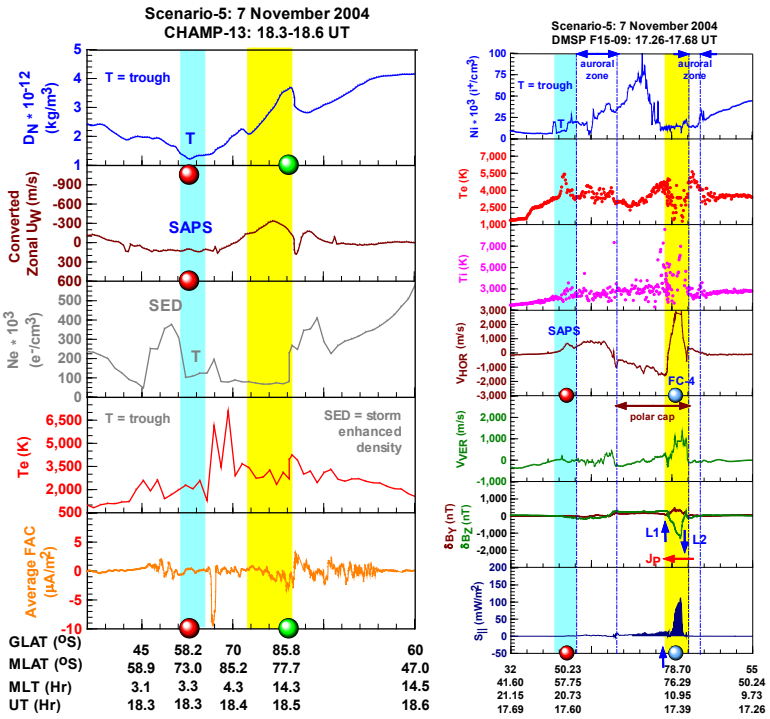

Figure 5.3: The development of localized neutral density increase (right panel) within the eroded polar cap region seemingly suggests weak I-T coupling. But the high-latitude X_H reconnection related FC-4 development, localized neutral density increase development within/above FC-4, and earthward energy deposition within FC-4 provide evidence of strong M-I-T coupling.

The strong erosion of high-latitude and polar cap plasma densities was caused by strong sub-auroral polarization streams (SAPS) electric (E) fields. During this shock-sheath driven 7-8 November 2004 Superstorm, the action of large storm-time SAPS FCs (V_{HOR}≈5,500 m/s) and associated SAPS E fields contributed to the erosion of plasmaspheric plasma during the strong M-I-T coupling unfolding. This strong plasmaspheric erosion resulted in the depletion of total electron content (TEC) at mid, high, and polar latitudes. Observational evidence is provided by our GPS TEC map series and matching CHAMP neutral density (Ne) and electron temperature (Te) line plot sets. Overall, these observations show plasmaspheric erosion events occurring in the longitude sector of the dayside Equatorial Ionization Anomaly (EIA) during the second half of the storm main phase and driven by the combination of strong convection and large storm-time SAPS E fields. Large SAPS FCs had been present since the initial phase.

Here, we show Figure 5.4 constructed with GSP TEC maps and pole-to-pole CHAMP Ne and Te line plots. These show the EIA appearing with a SED feature on the equatorward side of the electron density drop (i.e. signature of the plasmapause (PP) where Te peaked) and the depleted plasma density on the PP's poleward side. These observations also demonstrate that the enhanced polar convection moved the co-rotation/convection boundary inward or equatorward and caused -along with the strong SAPS E field- the erosion of the mid-latitude ionosphere and outer plasmasphere.

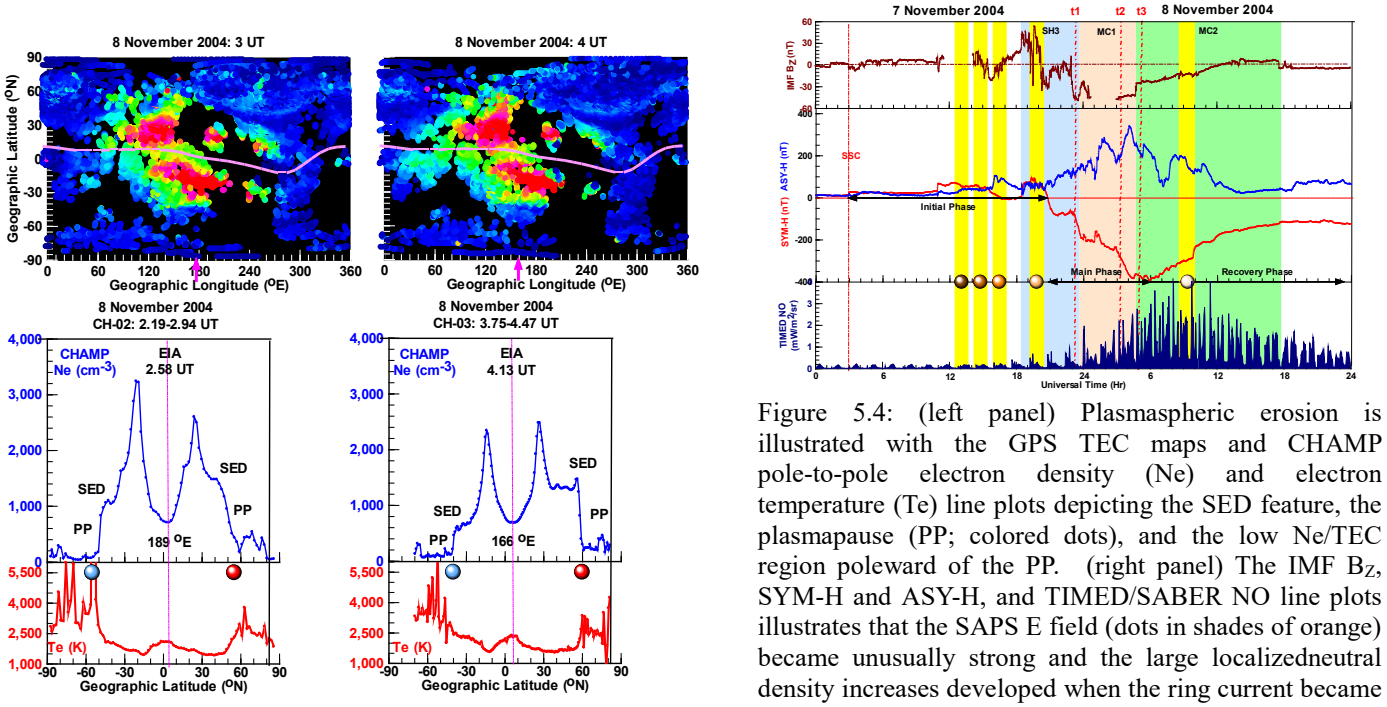

Figure 5.4: (left panel) Plasmaspheric erosion is illustrated with the GPS TEC maps and CHAMP pole-to-pole electron density (Ne) and electron temperature (Te) line plots depicting the SED feature, the plasmapause (PP; colored dots), and the low Ne/TEC region poleward of the PP. (right panel) The IMF B_Z, SYM-H and ASY-H, and TIMED/SABER NO line plots illustrates that the SAPS E field (dots in shades of orange) became unusually strong and the large localizedneutral density increases developed when the ring current became strongly asymmetric and while the NO content increased.

Conclusions:

Our new findings are as follows. (1) Strong M-I-T coupling was apparent when the localized neutral density (D_N) increases developed within/over FCs during FTEs and near the SED plume where electron density (Ne) increases also occurred. (2) M-I-T coupling was still strong but less apparent when the localized D_N increases developed within/over FCs during FTEs and in the eroded polar cap where Ne became depleted and thus Ne increases were absent. (3) Due to plasmaspheric erosion, driven by the combination of strong convection E field and large storm-time SAPS E fields -implied by the large SAPS FCs (~3,000-5,000 m/s) detected- and not by the thermospheric composition of low O/N_2 and high NO, the high-latitude Ne and TEC became decreased poleward of the PP. The reason is that a shock-sheath driven storm, like the 7-8 November 2004 Superstorm, leads to strong asymmetric ring current development -via the strong solar-wind convection E field- and thus to the development of strong storm-time SAPS E field (driving large SAPS FC), and the combination of these different E fields erode the plasmasphere.

(6) Horvath, I., & Lovell, B. C. (2020b). Investigating the development of distinctive Sub-Auroral Polarization Streams (SAPS) features impacted by large-scale Travelling Ionospheric Disturbances (TIDs) during the 7-8 November 2004 Superstorm *Journal of Geophysical Research: Space Physics* (under review)

Introduction:

During magnetic storms, Joule heating can take 50% of the total energy input. One the significant consequences of Joule heating deposition to the high-latitude coupled ionosphere-thermosphere (I-T) system is the production of atmospheric gravity waves (AGWs) in the neutral atmosphere (Richmond, 1978) launching travelling ionospheric disturbances (TIDs) in the ionosphere that travel both equatorward and poleward from the source region (Balthazor & Moffett, 1999). Associated thermospheric wind effects are such that downward drifts are induced by the prevailing eastward directed early evening winds in those longitude sectors where the declination angle is eastward or positive. As a result of enhanced TID-related downward drifts, the plasma density trough becomes deepened by mechanical wind effects. Thus, the trough becomes shifted to lower heights where the trough acquires a more molecular composition (He et al., 2011).

The aim of this study is to investigate the various types of sub-auroral flow channels developed under superstorm conditions during the 7-8 November 2004 Superstorm. These include the large SAPS flow channels developed during the initial phase plus the large structured single-peak and double-peak SAPS flow channels developed during the recovery phase.

Based on the observational evidence presented, we explain the development of large SAPS flow channels with the combined actions of solar-wind convection E field and enhanced large-scale FACs, with the long-lasting dipolarization event unfolding during the initial phase, with the quick substorm current wedge (SCW) activations occurring during the recovery phase, and with the direct impacts of large-scale TIDs passing through the SAPS flow channel and other auroral (i.e. FC-0) and polar cap (i.e. FC-4) flow channels. Our TID-related new results add to the previous study of Mishin et al. (2012) reporting first the ability of combined high-power High-Frequency (HF) heating and SAPS launching AGWs and to the recent study of Zhang et al. (2019) reporting first the ability of SAPS influencing both TID propagation and TID excitation. Demonstrating the variability of M-I-T coupling and thus improving our understanding of the coupled M-I-T system's complexity, our scenarios demonstrate the ability of large-scale TIDs enhancing the sunward flows of (i) sub-auroral flow channel of SAPS and SAPS wave structures (SAPS-WS) and 2-Peak SAPS_WS, (ii) auroral return flows (FC-0), and (iii) cross-polar reverse flows (FC-4).

Balthazor, R. L., & Moffett, R. J. (1999). Morphology of large-scale traveling atmospheric disturbances in the polar thermosphere. *Journal of Geophysical Research*, *104(A1)*, 15–24..https://doi.org/10.1029/1998JA900039

He, M., Liu, L., Wan, W., & Zhao, B. (2011). A study on the nighttime midlatitude ionospheric trough. *Journal of Geophysical Research*, 116(A5), A05315. https://doi.org/10.1029/2010JA016252

Mishin, E., Sutton, E., Milikh, G., Galkin, I., Roth, C., & Frster, M. (2012). F2-region atmospheric gravity waves due to high-power HF heating and subauroral polarization streams. *Geophysical Research Letters, 39(11)*, L11101. https://doi.org/10.1029/2012GL052004

Richmond, A. D. (1978). Gravity wave generation, propagation, and dissipation in the thermosphere. *Journal of Geophysical Research, 83(A9),* 4131–4145. https://doi.org/10.1029/JA083iA09p04131

Zhang, S.-R., Erickson, P. J., Coster, A. J., Rideout, W., Vierinen, J., Jonah, O. F., & Goncharenko, L. P. (2019). Subauroral and polar traveling ionospheric disturbances during the 7–9 September 2017 storms. *Space Weather, 17*. https://doi.org/10.1029/2019SW002325

Results:

During this study, we investigated the development of large sub-auroral polarization streams flow channels (SAPS FCs; ~5,000 m/s), and their further enhancement by large-scale travelling ionospheric disturbances (TIDs) and structuring into a single-peak wave structure (SAPS_WS; ~4,000 m/s) and a two-peak formation (2P-SAPS_WS; ~4,000 m/s) during the 7-8 November 2004 Superstorm by utilizing multi-satellite and multi-instrument measurements from the magnetosphere and topside ionosphere. A series large SAPS flow channels (FCs) -developed during a long-lasting dipolarization event- was further enhanced by large-scale travelling ionospheric disturbances (TIDs). These TIDs enhanced the SAPS FCs' sunward drifts directly by their own sunward drift surges and indirectly by the TIDs-related downward drift surges deepening the trough and thus enhancing the SAPS E fields via feedback mechanisms.

Here, in Figure 6.1, we show with a series of DMSP F16 scenarios the large-scale TIDs' sunward and downward drift surges developed prior to the first appearance of the large SAPS FC (left panel) of our interest, as indicated by the zero zonal and vertical drift velocities in the trough region (shaded interval in yellow). As indicated by the SAPS FC-related downward drift that is a TID signature, the SAPS FC's zonal drift became enhanced by the TIDs-related sunward drift surges when the large-scale TIDs passed through the SAPS FC, while the TIDs-related downward drift surges deepened the tough and thus increased the SAPS E field (middle panel). Large-scale TIDs propagating through the SAPS FC and auroral zone are most apparent in our Sc-4 (right panel).

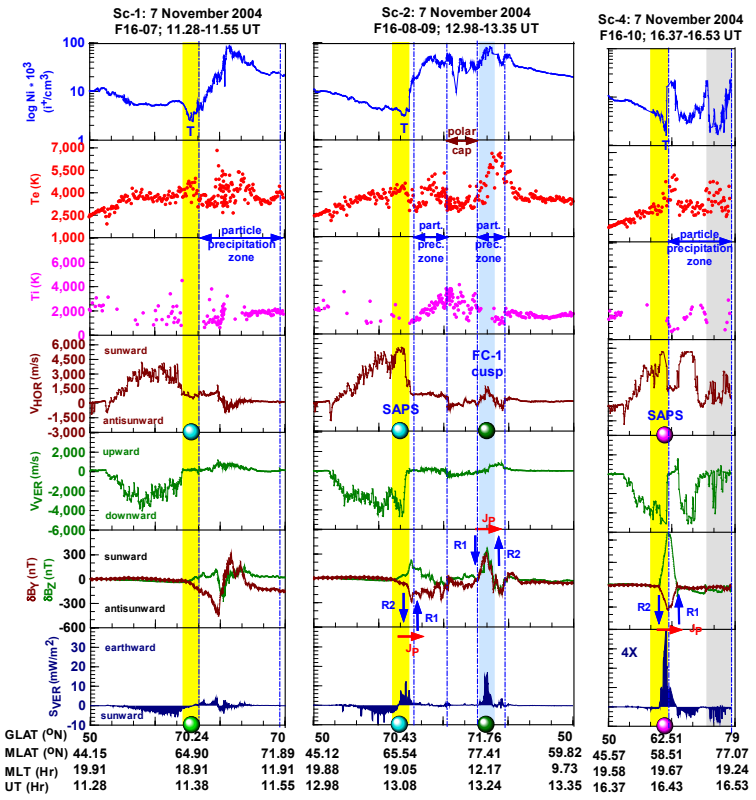

Figure 6.1: The F16 polar cross sections are constructed with ion density (Ni), electron and ion temperature (Te, Ti), cross-track ion drifts (V_{HOR}, V_{VER}), magnetic deflection components (δB_Y; δB_Z), and Poynting flux (S_{VER}) data. These scenarios illustrate TID related drift surges in the absence (Sc-1) and presence (Sc-2 and Sc-4) of large SAPS flow channels that developed in a short-circuited system acting as a current generator during dayside reconnection at low-latitude (FC-1 in Sc-2) and high-latitude (type-2 eastward flow channel (E-FC) in Sc-3).

In Figure 6.2, we show a series of Polar detections (left panel) revealing that these large SAPS FCs (dots and shaded intervals) developed during a long-lasting (~6 hours) dipolarization event associated with the formation of substorm current wedge (SCW). Meanwhile, the LANL electron and proton flux measurements (right panel) illustrate substorm injections, while the angle of azimuth time series depicts the azimuthal distribution of protons showing spreading when Sc-2—Sc-5 occurred, and thus implying the diversions of protons on either side of the tail region.

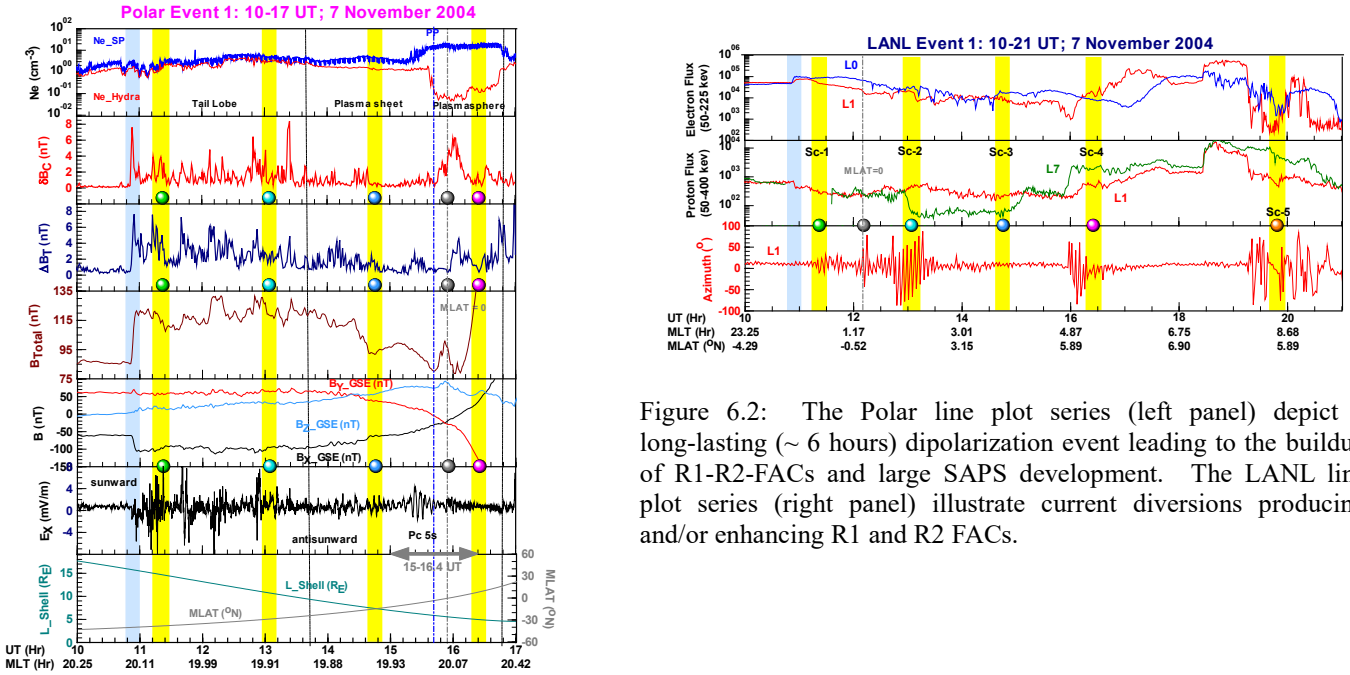

Figure 6.2: The Polar line plot series (left panel) depict a long-lasting (~ 6 hours) dipolarization event leading to the buildup of R1-R2-FACs and large SAPS development. The LANL line plot series (right panel) illustrate current diversions producing and/or enhancing R1 and R2 FACs.

Our results show also that the development of a series large SAPS wave structures (SAPS_WS) became enhanced by large-scale TIDs, in a short-circuited system acting sometimes as a current generator like during a fast dipolarization event and sometimes as a voltage generator. Here, in Figure 6.3 (left panel), we show that the SAPS structuring occurred in the vicinity of the duskside Harang reversal (HR), a region where the most intense M-I coupling takes palace enhancing the R1-R2 FACs and implying the activation of the sub-storm current wedge (SCW). During this SCW activation, the SAPS FC developed quickly in the region of increasing ↓R2 FACs (i.e. in a short-circuited system acting as a current generator) and became structured due to the current instability delivered by the dipolarization front or pulse. We show also (middle and right panels) that the large-scale TIDs passed through and thus enhanced various sunward FCs: the SAPS FC that developed in a short-circuited system acting as a voltage generator, the auroral return flows (FC-0), and the polar reverse convection flows (FC-4). All these FCs show the same style of structuring and imply that structuring started in the polar cap, with the structuring of FC-4, and became convected to auroral and sub-auroral latitudes. Here, the structured SAPS developed with a single peak (middle panel) and double peaks (right panel), and commonly in the wide trough region covering ~17.5 geographic latitude degrees (middle panel), where the plasmapause (PP) appeared on the trough equatorward side. Thus, along with the entire trough region, these structured SAPS FCs were associated with open flux tubes that passed over the polar cap's open field line regime.

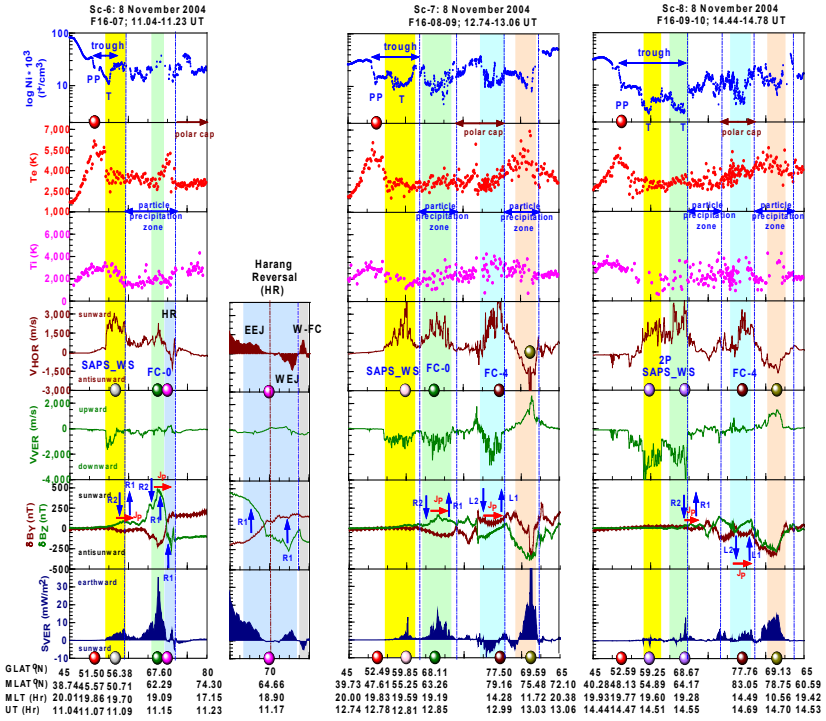

Figure 6.3: Scenarios 6-8 depict structured SAPS flow channels. These developed in a short-circuited system acting as a current generator (Sc-6) and voltage generator (Sc-7—Sc-8), and became enhanced by large-scale TIDs developed due to the energy deposition occurring at auroral latitudes. The single-peak SAPS wave structure (SAPS_WS) appeared with the Harang Reversal (HR) region implying ongoing dipolarization and associated sunbstorm current wedge (SCW) activation where the dipolarization pulse's earthward movement -by delivering current convective instability- led to SAPS structuring. Singe-peak and double-peak structured SAPS flow channels show structuring occurred in the polar region -by the structuring of FC-4- while structuring became convected to auroral and sub-auroral latitudes structuring FC-0 and SAPS respectively.

Conclusions:

Based on the observational evidence presented, we could unravel the development of these distinctive SAPS features. Our new results reveal the development of large SAPS features during the initial phase (Sc-2—Sc-5). Then, a series of dayside magnetopause reconnection events occurred that increased both the magnetospheric convection E field and the large-scale FACs while on the nightside a long-lasting (~6 hours) dipolarization event occurred of which long-lasting SCW formation produced a series of current diversions that led to the buildup of R1-R2 FACs and thus SAPS development during Sc-2—Sc-5 in a short-circuited system that acted as a current generator. During the recovery phase, when a quick SCW activation resulted in a quick ring current pressure buildup, the large SAPS feature developed during Sc-6 quickly in a short-circuited system that acted as a current generator and was structured due to the current instability delivered by the dipolarization pulse. Later on, during the recovery phase (Sc-7—Sc-8), the large single- and double-peak SAPS features developed in a short-circuited system that acted as a voltage generator. But SAPS structuring originated from the polar cap region with the structuring of cross-polar sunward flows of FC-4 that was convected to auroral and sub-auroral latitudes by the reverse polar convection and thus structured the auroral return flows (FC-0) and the SAPS flows.

Although these large and different types of SAPS features (SAPS, SAPS_WS, 2-Peak SAPS_WS) developed and appeared during the different storm phases, there was one common feature in their development. As our new results reveal, this is the presence of large-scale TIDs appearing as sunward and downward drift surges. As the large-scale TIDs passed through the various SAPS flow channels, each SAPS feature was associated with a downward drift that we specified as a TID signature and that was similar in magnitude as the SAPS feature's sunward zonal drift. Our new results reveal also that the large-scale TIDs, by passing through the SAPS flow channels and other sunward flows such as auroral return flows (FC-0; Sc-7) and cross-polar reverse flows (FC-4; Sc-7), significantly and positively impacted the development and maintenance of these distinctive large SAPS flows and sunward flows (FC-0, FC-4). The large-scale TIDs' sunward drift surges directly increased the SAPS, FC-0, and FC-4 flow channels' sunward zonal drifts. Meanwhile, indirectly -via feedback mechanisms- the large-scale TIDs' downward drift surges increased these flow channels' respective polarization E fields by deepening the plasma density within the trough.

(7) Horvath, I., & Lovell, B. C. (2020c). Dayside reconnection and energy deposition observed by CHAMP and DMSP and modelled by OpenGGCM during the 31 August 2005 moderate geomagnetic storm. *Planetary and Space Science* (under review)

Introduction:

The spatial structure of dayside magnetopause reconnection depends on the polarity of the north-south B_Z component and can occur in two major modes. When B_Z turns and remains southward, dayside magnetopause reconnection occurs at lower latitudes where the lower latitude reconnection X line (i.e. X_L) is situated at subcusp magnetopause latitudes and becomes greatly enhanced and thus the cusp region moves equatorward (Dungey, 1961). However, when B_Z points northward, dayside magnetopause reconnection occurs at higher latitudes where the higher latitude reconnection X line (X_H) is located at mantle/lobe magnetopause latitudes and thus tailward of the cusp (Dungey, 1963).

Meanwhile, the east-west B_Y component can introduce a strong dawn-dusk asymmetry where the northern-hemisphere cusp position is shifted to postnoon during $B_Y>0$ and prenoon during $B_Y<0$. Opposite scenarios occur in the Southern Hemisphere. Thus, the IMF B_Y component introduces an asymmetry about the noon-midnight meridian into the X_L and X_H reconnection processes, and these asymmetries also impact the patterns of polar convection, magnetic deflection, auroral precipitation, and large-scale FACs (e.g. Sandholt et al., 2006 and references therein).

Regarding the X_L and X_H reconnection events' related particle precipitation regimes, magnetosheath plasma injections trigger the development of their respective type-1 and type-2 aurorae that are the two main categories of poleward moving auroral forms (PMAFs; Fasel et al., 1994).

In this study, we focused on the 31 August 2005 geomagnetic storm in order to investigate (i) the Challenging Minisatellite Payload (CHAMP) detected neutral density spikes and their neutral density and electron density environments, to identify (ii) these density spikes' associated dayside low-latitude X_L and high-latitude X_H magnetopause reconnection events and (iii) the X_L and X_H reconnection signatures appearing both in particle precipitation and in FC, to investigate (iv) the electromagnetic energy deposition occurring within these FCs, and (v) to find out how realistically the Open Global General Circulation Model (OpenGGCM) performed in reproducing these energy deposition events and their various specific variables such as large-scale FACs and electric fields during two scenarios.

Dungey, J. W. (1961). Interplanetary magnetic field and the auroral zones. *Physical Review Lett*ers, *6(2)*, 47–48. https://doi:10.1103/PhysRevLett.6.47

Dungey, J. (1963). The structure of the exosphere or adventures in velocity space, in *Geophysics, The Earth's Environment*, edited by C. DeWitt, J. Hieblot, and A. Lebeau, pp. 505–550, Gordon & Breach, New York

Fasel, G., 1995. Dayside poleward moving auroral forms: A statistical study. *Journal of Geophysical Research, 100(A7),* 11,891-11,905. https://doi.org/10.1029/95JA00854

Sandholt, P. E., Dyrland, M., & Farrugia, C. J. (2006). Dayside aurorae and polar arcs under south-east IMF orientation. *Annales Geophysicae*, *24*, 3421-3432. https://doi.org/10.5194/angeo-24-3421-2006

Results:

The development of neutral density spike within/over an eastward flow channel (E-FC) during high-latitude X_H and low-latitude X_L magnetopause reconnection events. The significance of these results is that the E-FCs are less investigated and thus are less understood.

Here, in Figure 7.1, we show with correlated multi-satellite data the high-latitude X_H reconnection signatures tracked in the magnetosphere, topside ionosphere, and thermosphere. In the magnetosphere, this high-latitude X_H reconnection event was detected by the Polar satellite (top left and middle panels), which tracked the high-latitude X_H cusp and its underlying E-FC, while the high-latitude X_H cusp and its underlying E-FC were detected in the topside ionosphere by DMSP F15 (bottom left panel) and in the thermosphere by CHAMP (bottom right panel).

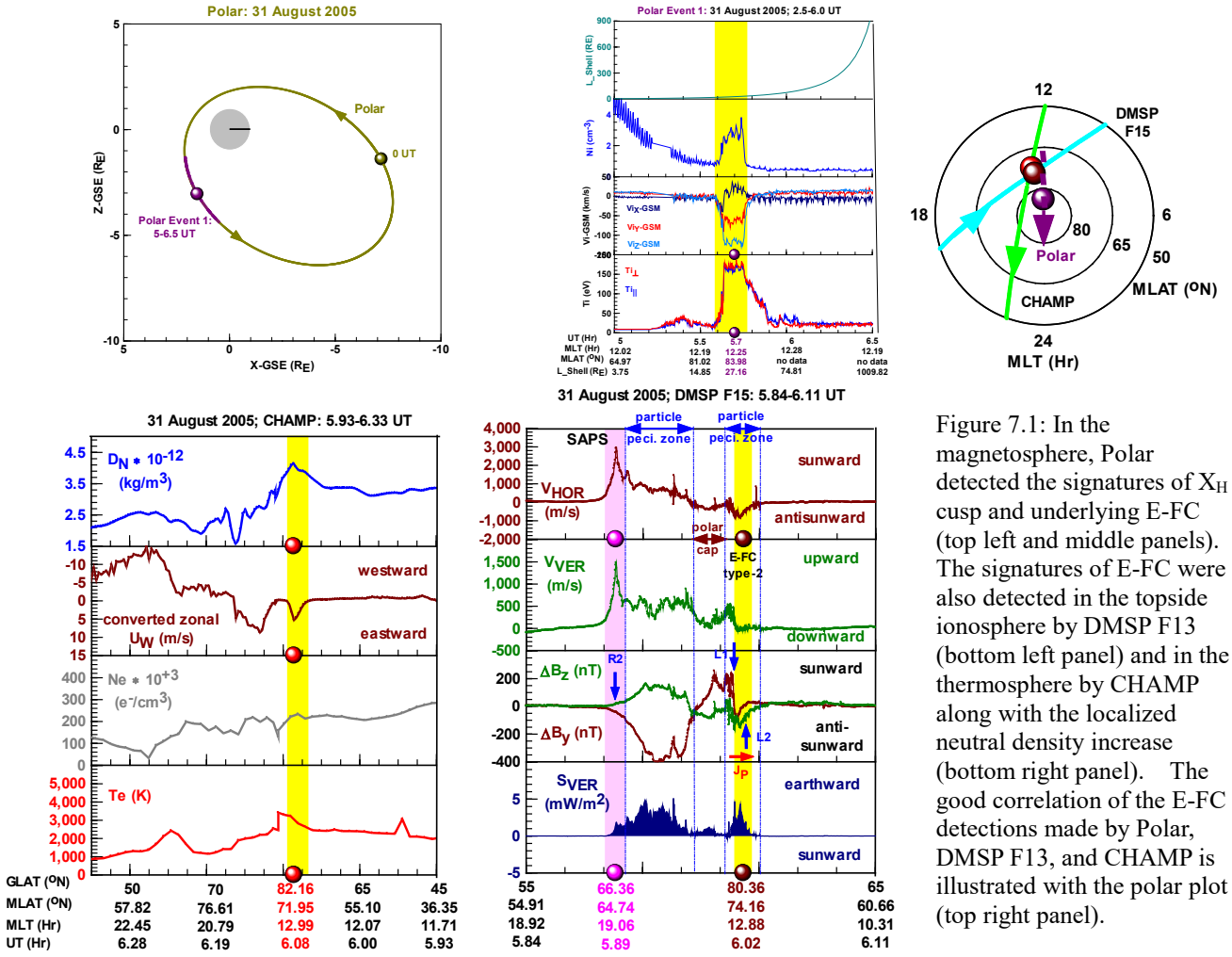

Figure 7.1: In the magnetosphere, Polar detected the signatures of X_H cusp and underlying E-FC (top left and middle panels). The signatures of E-FC were also detected in the topside ionosphere by DMSP F13 (bottom left panel) and in the thermosphere by CHAMP along with the localized neutral density increase (bottom right panel). The good correlation of the E-FC detections made by Polar, DMSP F13, and CHAMP is illustrated with the polar plot (top right panel).

The ability of Open Global General Circulation Model (OpenGGCM) to reproduce one of the X_H reconnection scenarios. OpenGGCM was able to reproduce the E-FC and related characteristics, since OpenGGCM is a complex model that solves resistive magnetohydrodynamic (MHD) equations with solar input and computes a 3D global magnetosphere and a 2D high-latitude ionosphere. The significance of these OpenGGCM simulations is that they further verify the accuracy of our E-FC and large-scale FAC interpretations and that these simulations can be used as a tool to better understand M-I-T coupling.

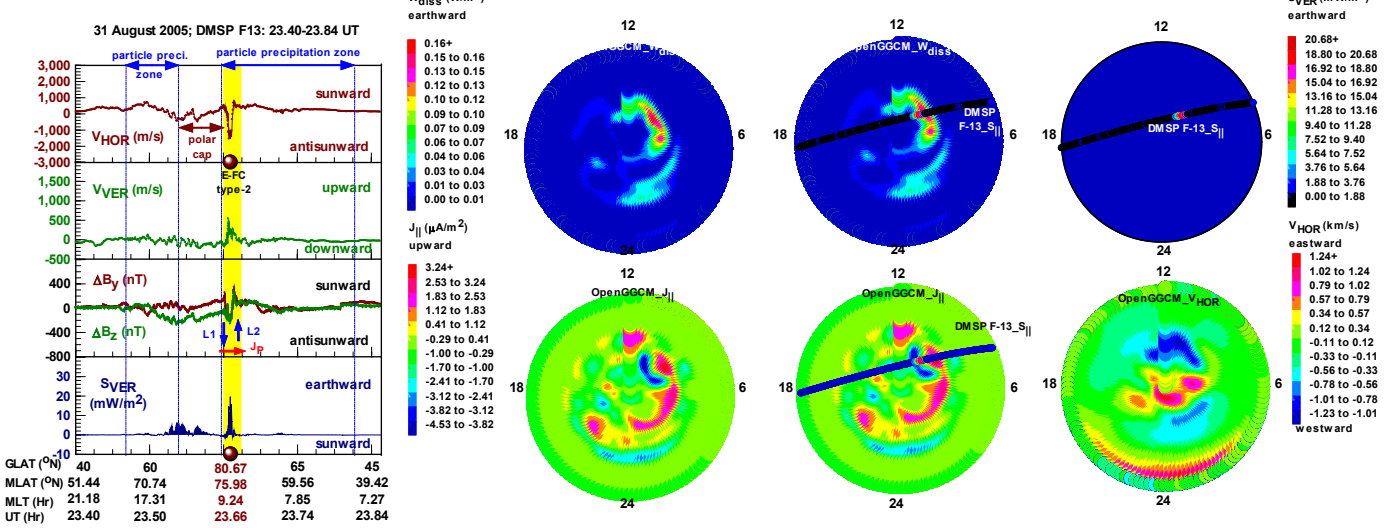

Figure 7.2: A high-latitude X_H reconnection event and associated E-FC where lobe currents connected (↓L1-↑L2 FACs) and earthward energy deposition detected by DMSP F13 (left panel) and reproduced by OpenGGCM (right panel).

Here, in Figure 7.2 we show another high-latitude X_H reconnection event tracked by DMSP F13 in the topside ionosphere (left panel) that we compare with OpenGGCM simulations (right panel). But we focus on some specific details such as the location of earthward energy deposition (measured by the Poynting flux; S_{VER}), the pattern of lobe (L) currents (↓L1-↑L2 FACs) connecting with equatorward Pedersen currents of which eastward electric field drove the antisunward flows of the E-FC. The top right panel of Figure 7.2 shows that OpenGGCM simulated the larger region of enhanced Joule heating rates in the midday sector covering the region of DMSP F13 detected earthward directed Poynting flux. But the bottom right panel of Figure 7.2 shows some specific details. These include the oppositely directed large-scale FACs that we specified as lobe currents. OpenGGCM simulated these lobe currents where DMSP F13 detected the E-FC and with the same pattern (i.e. ↓L1 on the poleward side and ↑L2 on the equatorward side), and the eastward (or antisunward) drift of the E-FC.

The development of neutral density spike within/over a FC-2 during a low-latitude X_L magnetopause reconnection event driven externally by the antisunward propagating solar-wind Alfven waves while a high-latitude X_H magnetopause reconnection event was unfolding. The significance of these results is that they demonstrate simultaneously occurring X_L and X_H reconnection events and explain their respective earthward and sunward energy depositions.

Here, in Figure 7.3, we show that ACE on the dayside (left panel) detected solar-wind Alfven waves as the scatter plots show (middle panel) and periodic B_Z variations (right panel) that are similar to the periodic B_Y variations detected by Cluster_C3 (right panel) on the nightside (left panel).

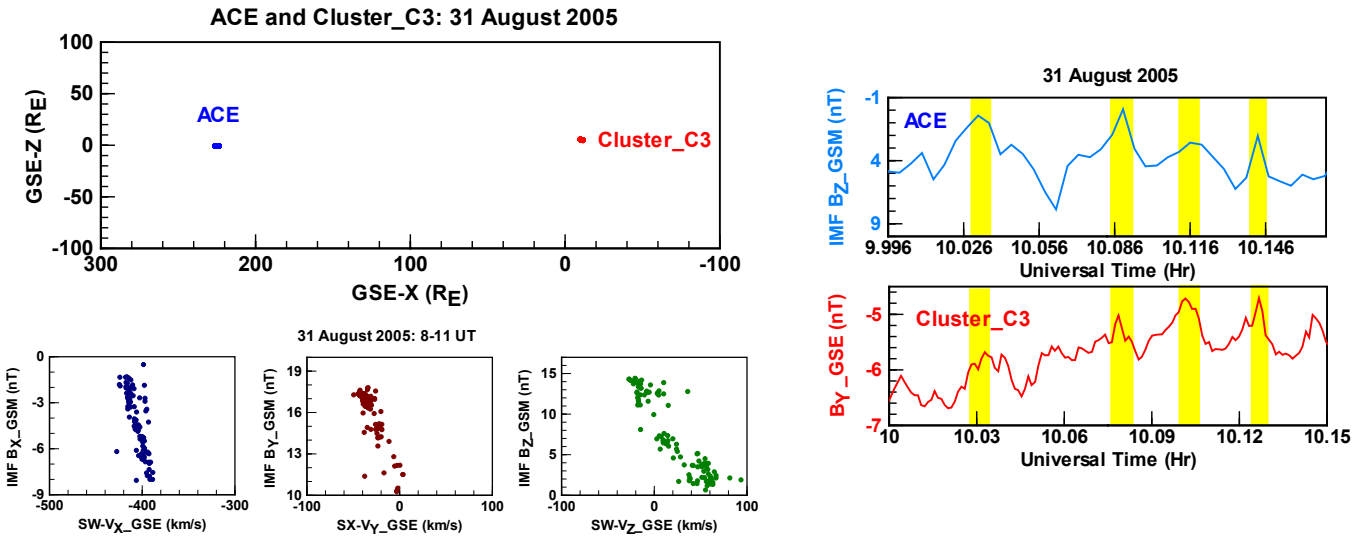

Figure 7.3: ACE on the dayside and Cluster_C3 on the nightside (left panel) detected periodic B field variations (right panel) in the presence of solar-wind Alfven waves (middle panel).

We show also with our DMSP F13 scenario in Figure 7.4 that these periodic magnetospheric B field fluctuations (top left panel) also occurred -during the X_L reconnection event triggered externally by the solar-wind Alfven waves- in the topside ionosphere (bottom left panel) and led to the development of DP-2 amplitudes seen both in the topside vertical drift data (bottom left panel) and in the B_X component ground-based magnetometer data (top right panel). Solar-wind Alfven waves led to earthward energy deposition within FC-2 and sunward energy deposition within FC-4 (bottom left panel) developing during the prevailing X_H reconnection. But the localized neutral density increase developed within/over FC-2 where the energy deposition was earthward (bottom right panel).

Conclusions:

From these findings we conclude for this moderate 31 August 2005 geomagnetic storm (1) the regular development of X_H reconnection related type-2 E-FC (at $B_Z>0$ and $B_Y\leq 0$), which is less investigated and therefore less understood compared to the sunward E×B convection flows (i.e. FC-4) occurring at $B_Z>0$ and $B_Y>0$ and (2) the significant role of antisunward propagating solar-wind Alfvén waves (i) leading to sunward electromagnetic energy deposition within FC-4 that is very different from the expected B_Y-dominated near-cusp earthward energy deposition scenario well documented in various previous studies, (ii) driving externally X_L reconnection during a prevailing X_H reconnection event and (iii) leading to the development of FC-2 during this X_L reconnection event and to earthward electromagnetic energy deposition within this FC-2.

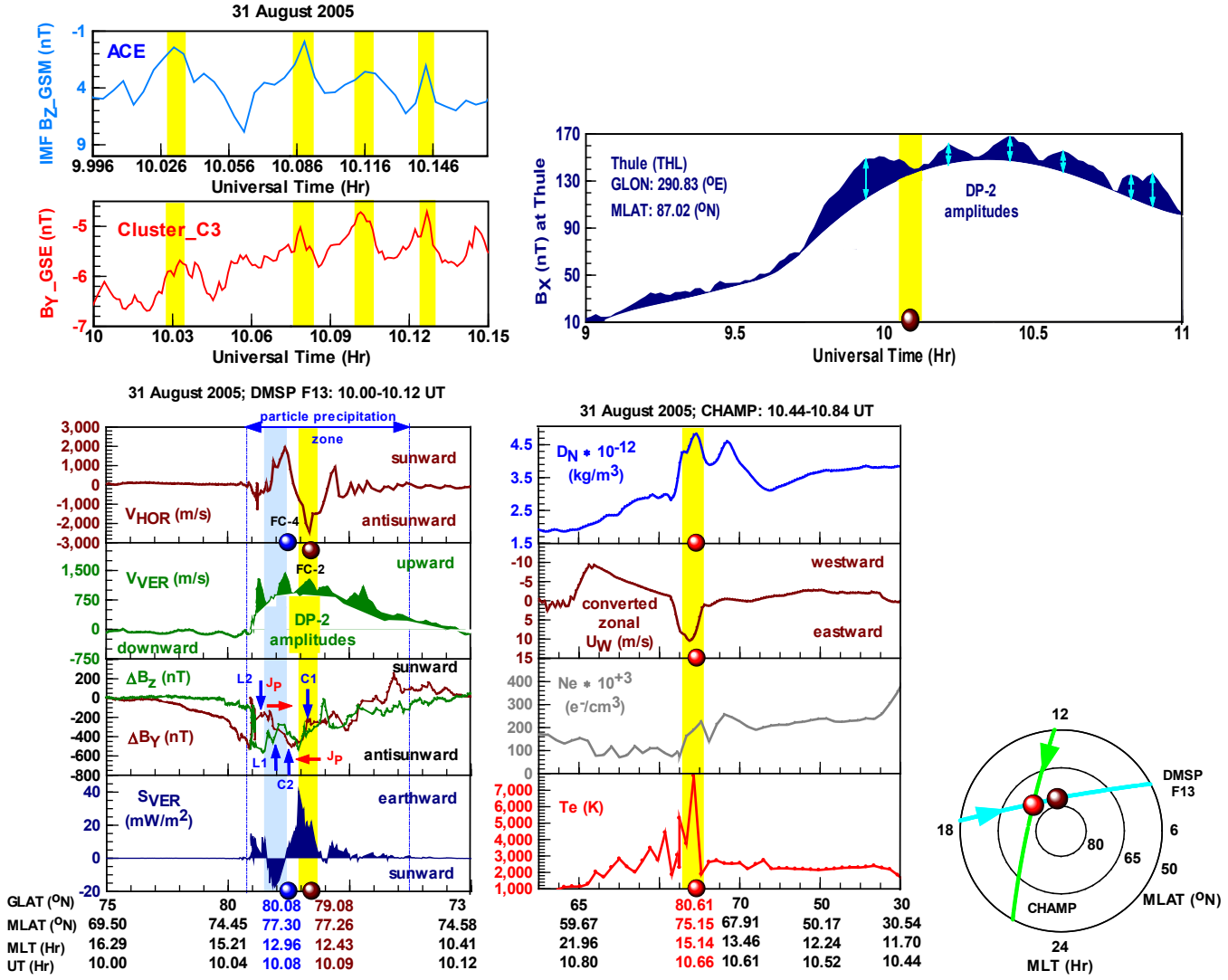

Figure 7.4: Our scenarios (bottom panels) illustrates simultaneously occurring X_H reconnection under the prevailing IMF B_Z>0 conditions and its related FC-4, X_L reconnection triggered externally by the solar-wind Alfven waves present and its related FC-2 where the neutral density increased locally, and of B field fluctuations (top panels) causing the development of DP-2 amplitudes.

List of Publications and Significant Collaborations that resulted from your AOARD supported project

a) papers published in peer-reviewed journals:

1) Journal name: *Journal of Geophysical Research: Space Physics, 123(8),* 6760-6775.
Title: Investigating high-latitude energy deposition events occurring during the 17 January 2005 geomagnetic storm.
Authors: Horvath and Lovell (2018a)
https://doi.org/10.1029/2018JA025465 Horvath, I., & Lovell, B. C. (2018a
Date of online publication: 11 AUG 2018

2) Journal name: *Journal of Geophysical Research: Space Physics, 123(9),* 7806-7824.
Title: Polar ion temperature variations during the 22 January 2012 magnetic storm.
Authors: Horvath and Lovell (2018b)
https://doi.org/10.1029/2018JA025727
Date of online publication: 17 SEP 2018

3) Journal name: *Journal of Geophysical Research: Space Physics*, *124(1)*, 715-733
Title: Investigating the development of abnormal subauroral ion drift (ASAID) and abnormal subauroral polarization stream (ASAPS) during the magnetically quiet times of October 2003.
Authors: Horvath and Lovell (2019a)
https://doi.org/10.1029/2018JA026230
Date of online publication: 28 JAN 2019

4) Journal name: *Journal of Geophysical Research: Space Physics, 124(7)*, 6097-6116.
Title: Abnormal sub-auroral ion drifts (ASAID) and Pi2 pulsations observed by the Polar satellite during the magnetically quiet times of October 2003.
Authors: Horvath and Lovell (2019b)
https://doi.org/10.1029/2019JA026725
Date of online publication: 13 JUL 2019

b) papers published in peer-reviewed conference proceedings:
None
c) papers published in non-peer-reviewed journals and conference proceedings:
Non:
d) conference presentations without papers:
None
e) manuscripts submitted but not yet published:

1) Journal name: *Journal of Geophysical Research: Space Physics*
Title: Investigating Magnetosphere-Ionosphere-Thermosphere (M-I-T) coupling occurring during the 7-8 November 2004 Superstorm.
Authors: Horvath and Lovell (2020a)
Date received: 02 OCT 2019
Date accepted: 05 FEB 2020

2) Journal name: *Journal of Geophysical Research: Space Physics*
Title: Investigating the development of distinctive Sub-Auroral Polarization Streams (SAPS) features impacted by large-scale Travelling Ionospheric Disturbances (TIDs) during the 7-8 November 2004 Superstorm
Authors: Horvath and Lovell (2020b)
Date received: 16 JAN 2020

3) Journal name: *Planetary and Space Science*
Title: Dayside reconnection and energy deposition observed by CHAMP and DMSP and modelled by OpenGGCM during the 31 August 2005 moderate geomagnetic storm.
Authors: Horvath and Lovell (2020c)
Date received: 30 JAN 2020

f) provide a list any interactions with industry or with Air Force Research Laboratory scientists or significant collaborations that resulted from this work:

1. **Event Name:** AOARD/AFOSR GRANT REVIEW MEETING
   Venue: The University of Queensland, Brisbane, QLD, Australia
   Title: Investigating ionospheric and thermospheric variations during geomagnetic storms
   Date: 12 July 2018
   Presenter: Dr Ildiko Horvath

2. **Event Name:** 2018 Joint CEDAR-GEM Workshop,
   Venue: Eldorado Hotel and Spa and the Hilton Santa Fe Historic Plaza in Santa Fe, New Mexico
   Title: Coordinated Poynting Flux (PF) and neutral density enhancements
   Date: 24-29 June 2018
   Presenter: Dr Cheryl Huang, Senior Research Physicist
   AFRL/RVBXP, Kirtland AFB, NM, USA

3. **Event Name:** 2019 Joint CEDAR-GEM Workshop,
   Venue: Eldorado Hotel and Spa and the Hilton Santa Fe Historic Plaza in Santa Fe, New Mexico
   Title: MIT coupling captured by OpenGGCM
   Date: 16-21 June 2019
   Presenter: Dr Cheryl Huang, Senior Research Physicist
   AFRL/RVBXP, Kirtland AFB, NM, USA

4. **Email communications** with Dr E. Mishin Senior Research Physicist
   AFRL Space Vehicles Directorate: Kirtland AFB, NM, US

5. **Email communications** with Dr Cheryl Huang, Senior Research Physicist
   AFRL/RVBXP, Kirtland AFB, NM, USA